Kärhä, O.; Tanskanen, E. I.

Newly Digitized Data From Scandinavian Magnetometer Array Network Shows Large Regional Differences in Magnetic Environment

Published in:
Journal of Geophysical Research: Space Physics

DOI:
10.1029/2022JA030311

Published: 01/05/2022

Document Version
Publisher's PDF, also known as Version of record

AGU ADVANCING EARTH AND SPACE SCIENCE

JGR Space Physics

RESEARCH ARTICLE
10.1029/2022JA030311

Newly Digitized Data From Scandinavian Magnetometer Array Network Shows Large Regional Differences in Magnetic Environment

O. Kärhä[1] and E. I. Tanskanen[1,2]

[1]Sodankylä Geophysical Observatory, University of Oulu, Sodankylä, Finland, [2]Department of Electronics and Nanoengineering, Aalto University, Espoo, Finland

Key Points:

- A newly developed DigiMAG method enables the usage of magnetic data from the historical SMA network
- The horizontal differences reach more than 500 nT over a distance of 167 km in the vicinity of 65° (CGM) latitude
- In 3 min, 2.8 nT km−1 difference arise in the H-component time derivatives between two SMA stations

Correspondence to:

O. Kärhä,
otto.karha@oulu.fi

Citation:

Kärhä, O., & Tanskanen, E. I. (2022). Newly digitized data from Scandinavian magnetometer array network shows large regional differences in magnetic environment. *Journal of Geophysical Research: Space Physics*, *127*, e2022JA030311. https://doi.org/10.1029/2022JA030311

Received 21 JAN 2022
Accepted 16 APR 2022

Author Contributions:

Conceptualization: O. Kärhä
Data curation: O. Kärhä
Formal analysis: O. Kärhä, E. I. Tanskanen
Funding acquisition: O. Kärhä, E. I. Tanskanen
Investigation: O. Kärhä
Methodology: O. Kärhä
Project Administration: E. I. Tanskanen
Resources: O. Kärhä, E. I. Tanskanen
Software: O. Kärhä
Supervision: E. I. Tanskanen
Validation: O. Kärhä, E. I. Tanskanen
Visualization: O. Kärhä
Writing – original draft: O. Kärhä
Writing – review & editing: O. Kärhä

Abstract The International Magnetospheric Study (IMS) took place from 1977 to 1979. An objective was to study the magnetosphere at different heights on the Earth and in space simultaneously. The Scandinavian Magnetometer Array (SMA), where a dense magnetometer array was placed in the northern part of Scandinavia, was part of the IMS. This array extended 1,570 km in north-south and 1,290 km in east-west directions. The SMA-magnetometers contained a camera with 35 mm film and three wire-suspended magnets. These instruments recorded the movement of the magnets optically on the film. The usability of the SMA data has been limited by time-consuming digitization by hand. Thus, most of the recordings has been left nondigitized and unstudied. We have developed a method, named DigiMAG, to digitize the SMA recordings by using a custom-built device. This article presents the high-latitude dynamics of the strongest magnetic storm in 1977 between October 26 and 30. We analyze newly digitized data from Rostadalen (ROS), Evenes (EVE), Ritsemjokk (RIJ), and Kiruna (KIR) stations for the three storm-time substorms on October 26–29, 1977. The results show that in the vicinity of the 65° latitude, the storm-time differences of horizontal magnetic components can exceed 500 nT. During the recovery phase of a substorm, 2.8 nT km^{-1} difference arises over a distance of 167 km between the H-component time derivatives of ROS and RIJ stations in 3 minutes.

1. Introduction

The Earth has a magnetic field that protects it from particles coming from the Sun and interstellar sources. Changes in solar wind properties and the magnetosphere's response to these changes cause geomagnetic activity. This activity occurs mainly as magnetic storms (Gonzalez et al., 1994) and substorms (E. I. Tanskanen, 2009). A major magnetic storm can break down communication satellites and interrupt electric power networks (Pirjola, 1989). The best way to learn to understand the magnetic field and related phenomena is to measure its changes. In 1960s, researchers presented the idea that magnetometer stations could be installed in a dense chain in a north-south direction. The concept of the Alaskan meridian chain was introduced in 1968. This chain proved the presence of the auroral oval and its poleward expansion (Akasofu et al., 1971, 1973, 1980; Snyder & Akasofu, 1972). The inadequacy of the meridian chain is that it cannot be used to properly study phenomena moving in an east-west direction.

The Scandinavian Magnetometer Array (SMA) was part of the International Magnetospheric Study 1977–1979 (IMS). The total number of the SMA stations was 42, 6 provided by the Technical University of Braunschweig, the other 36 by the University of Münster. This article focuses on the SMA stations from the University of Münster locating in Scandinavia and extending both in north-south and east-west directions. The SMA-instruments were based on modified Gough-Reitzel type magnetometers. These instruments contained a camera with 35 mm film and three wire-suspended magnets. The movement of the magnets was recorded optically on the film. The SMA stations recorded a considerable amount of data (Baumjohann, 1982; Küppers et al., 1979; Untiedt & Baumjohann, 1993). Researchers found that the value of the data is limited by time-consuming digitization by hand (Araki et al., 1992; Küppers et al., 1979).

The Auroral Electrojet (AE) indices are derived from the variations of the horizontal component of the geomagnetic field in the auroral zone (Davis & Sugiura, 1966). The year 1977 is the only full year for which the AE index has not been produced since 1957. Although the collection of the data from the magnetometer film recordings is time-consuming, the new DigiMAG method makes it possible to digitize the missing high-latitude geomagnetic data and fill the otherwise continuous AE index data series since July 1957 to July 1988. This article presents

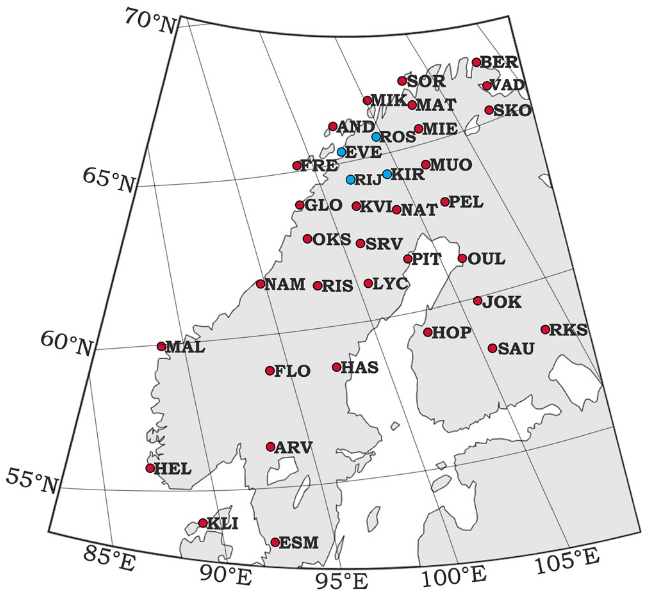

Figure 1. SMA station map in corrected geomagnetic coordinates (CGM) for the year 1977. The circles show the locations of the SMA stations from the University of Münster. The stations marked in blue were around the permanent AE magnetometer station Abisko (ABK) and are under study in this article. Over 60° (CGM) latitude, on average approximately, the distance between the stations in north-south direction was 125 km and in east-west direction 155 km.

the newly digitized data from the high-latitude SMA stations for the largest geomagnetic storm in 1977. According to the lowest Dst peak value, the digitized storm interval is the fourth largest during the IMS and the sixth largest during the entire SMA operation interval. The SMA stations used here are selected such that the digitized data can be used as AE data, and thus filling the missing data for AE indices. The results of this article are compared with data from a permanent magnetometer station Abisko (ABK). We have developed a new method named "a positive-negative derivative (PdNd)" which enables comparison of rapid magnetic field changes during substorm expansion phase.

2. Scandinavian Magnetometer Array, Instruments, and Recordings

2.1. SMA Network

Coordinated simultaneous multimethod IMS measurements at different altitudes were seen as an advantage of the SMA over other magnetometer array field operations (Küppers et al., 1979; Pellinen et al., 1982; P. Tanskanen et al., 1982). The assumption was that electrojets flowing in parallel to the magnetic oval would predominate. Thus, the SMA station's locations formed direct chains approximately toward the magnetic north. These locations are shown in Figure 1, and the coordinates are given in Table 1. The SMA instruments were buried vertically on the ground, primarily to locations where the static magnetic field gradient was low. This reduced the errors in declination measurements with the compass theodolite (Küppers et al., 1979).

At the high latitude, the dense array extended from western Norway to the Soviet Union. At lower latitudes, the distance between the stations increased, especially in the magnetic north-south direction. During the IMS, there were temporary and permanent magnetometer stations in the Scandinavian region. Temporary stations came from the Institute of Geophysics, the University of Münster, the Technical University of Braunschweig, the Polar Geophysical Institute at Apatity, and the Geomagnetism Unit of the UK Institute of the Geological Sciences. Permanent stations were Ny-Ålesund (NAL), Bear Island (BJN), Tromsø (TRO), Abisko (ABK), Loparskaya (LPY), Lovozero (LOZ), Sodankylä (SOD), Dombås (DOB), Nurmijärvi (NUR), Lovö (LOV), and Leningrad (LNN) (Green, 1981; Küppers et al., 1979; Maurer & Theile, 1978; Stuart, 1982).

After the IMS ended in 1979, the EISCAT magnetometer cross began operating in northern Scandinavia in 1982. This magnetometer cross was a joint operation of the Technical University of Braunschweig, Sodankylä Geophysical Observatory (SGO), Finnish Meteorological Institute (FMI), and the University of Tromsø. Initially, the cross consisted of the following five stations: Sørøya (SOR), Alta (ALT), Kautoketo (KAU), Muonio (MUO), and Pello (PEL). Kilpisjärvi (KIL) and Kevo (KEV) joined to the cross in 1983 (Lühr et al., 1984). ALT and KAU stations were removed from the cross in 1990 before the current IMAGE network began operating in 1991. Figure 2 shows the stations of different magnetometer arrays that were located in the vicinity of the AE station at Abisko. The magnetic longitude of ABK has changed nearly 4° since the SMA measurements. The SMA network had the densest station spacing around the AE station. Subsequent arrays have no stations within a radius of 200 km in the magnetic west, magnetic north, or the area between these directions. Only the SMA array has recorded existing data on the proximity of these directions. The data provides information on changes in the magnetic field over a short distance in the vicinity of the 65° latitude.

2.2. Type Münster Gough-Reitzel Magnetometer

The standard Gough-Reitzel magnetometers were designed for field use. Except for a battery, the components were installed inside an airtight tube. The unit price of a portable magnetometer was under $1,500 in 1967, which is equivalent to $11,600 in 2020 due to inflation. When the tube is buried in the ground, temperature-sensitive magnets and torsion wires are at a depth of 1.5 m or more. At this depth, the temperature gradient is no more

Table 1
SMA Station List

Symbol	Name	CGM coord. 1977		Geographic coord.		Start date	End date
		Lat.	Long.	Lat.	Long.		
SOR	Söröya	67.02	107.99	70.60	22.22	11 October 1975	20 March 1980
BER	Berlevag	66.83	113.29	70.85	29.13	08 September 1976	26 October 1979
MIK	Mikkelvik	66.72	105.16	70.07	19.03	03 August 1974	12 February 1980
MAT	Mattisdalen	66.23	107.79	69.85	22.92	10 October 1975	18 March 1980
AND	Andenes	66.18	102.23	69.30	16.02	22 September 1976	12 September 1979
VAD	Vadsö	66.07	113.00	70.10	29.65	07 September 1976	25 October 1979
ROS	Rostadalen	65.57	104.59	68.97	19.67	04 August 1974	14 February 1980
MIE	Mieron	65.47	107.39	69.12	23.27	10 October 1975	17 March 1980
SKO	Skogfoss	65.36	112.22	69.37	29.42	07 September 1976	22 September 1979
EVE	Evenes	65.34	102.08	68.53	16.77	23 September 1976	11 February 1980
FRE	Fredvang	65.18	99.04	68.08	13.17	22 September 1976	09 February 1980
RIJ	Ritsemjokk	64.45	101.93	67.70	17.50	02 September 1976	15 March 1980
KIR	Kiruna	64.37	104.22	67.83	20.42	07 December 1974	15 March 1980
MUO	Muonio	64.36	106.74	68.03	23.57	10 October 1975	04 June 1980
GLO	Glomfjord	63.94	98.38	66.90	13.58	15 October 1975	07 February 1980
KVI	Kvikkjokk	63.60	101.63	66.90	17.92	01 September 1976	13 March 1980
NAT	Nattavaara	63.24	103.84	66.75	21.00	01 August 1974	07 January 1980
PEL	Pello	63.10	106.76	66.85	24.73	09 October 1975	24 February 1980
OKS	Okstindan	62.86	98.14	65.90	14.27	20 September 1976	06 February 1980
SRV	Storavan	62.44	101.02	65.78	18.18	26 September 1976	17 February 1980
PIT	Pitea	61.67	103.27	65.25	21.58	02 August 1974	15 February 1980
NAM	Namsos	61.62	94.76	64.45	11.13	18 September 1976	04 February 1980
RIS	Risede	61.35	97.84	64.50	15.13	19 September 1976	05 February 1980
OUL	Oulu	61.29	106.20	65.10	25.48	06 October 1975	19 June 1980
LYC	Lycksele	61.16	100.60	64.57	18.68	27 September 1976	17 February 1980
JOK	Jokikylä	59.89	105.94	63.77	26.13	06 October 1975	23 February 1980
MAL	Malöy	59.80	88.73	62.18	5.10	17 September 1976	05 September 1979
HOP	Hööpaka	59.30	102.70	63.01	22.56	14 July 1978	15 June 1980
FLO	Flötningen	58.83	94.01	61.88	12.23	06 July 1978	26 February 1980
HAS	Hassela	58.71	97.43	62.07	16.50	27 September 1976	27 September 1979
RKS	Röksä	58.47	108.64	62.57	30.26	12 July 1978	12 October 1979
SAU	Sauvamäki	58.36	105.59	62.30	26.65	05 October 1975	16 June 1980
ARV	Arvika	56.36	93.09	59.60	12.60	14 September 1976	25 February 1980
HEL	Hellvik	55.77	87.23	58.52	5.77	15 September 1976	02 September 1979
KLI	Klim	53.92	89.22	57.12	9.17	26 August 1976	01 September 1979
ESM	Esmared	53.20	92.26	56.74	13.22	03 July 1978	28 February 1980

Note. The symbol, name, and geographic coordinates (GCS) are adopted from (Küppers et al., 1979). CGM coordinates are calculated according to (Gustafsson, 1970; Tsyganenko et al., 1987). A start date indicates the beginning of the first measurement interval and end date the closing of the last interval.

than 0.1°C/week (Gough & Reitzel, 1967). Field operation experience has shown that temperature compensation also works in north Scandinavia if ground contact is sufficient. The SMA instruments were based on modified Gough-Reitzel magnetometers with a 35 mm film camera and three wire-suspended magnets (Baumjohann, 1982; Küppers et al., 1979). This second-generation Gough-Reitzel magnetometer was called type Münster

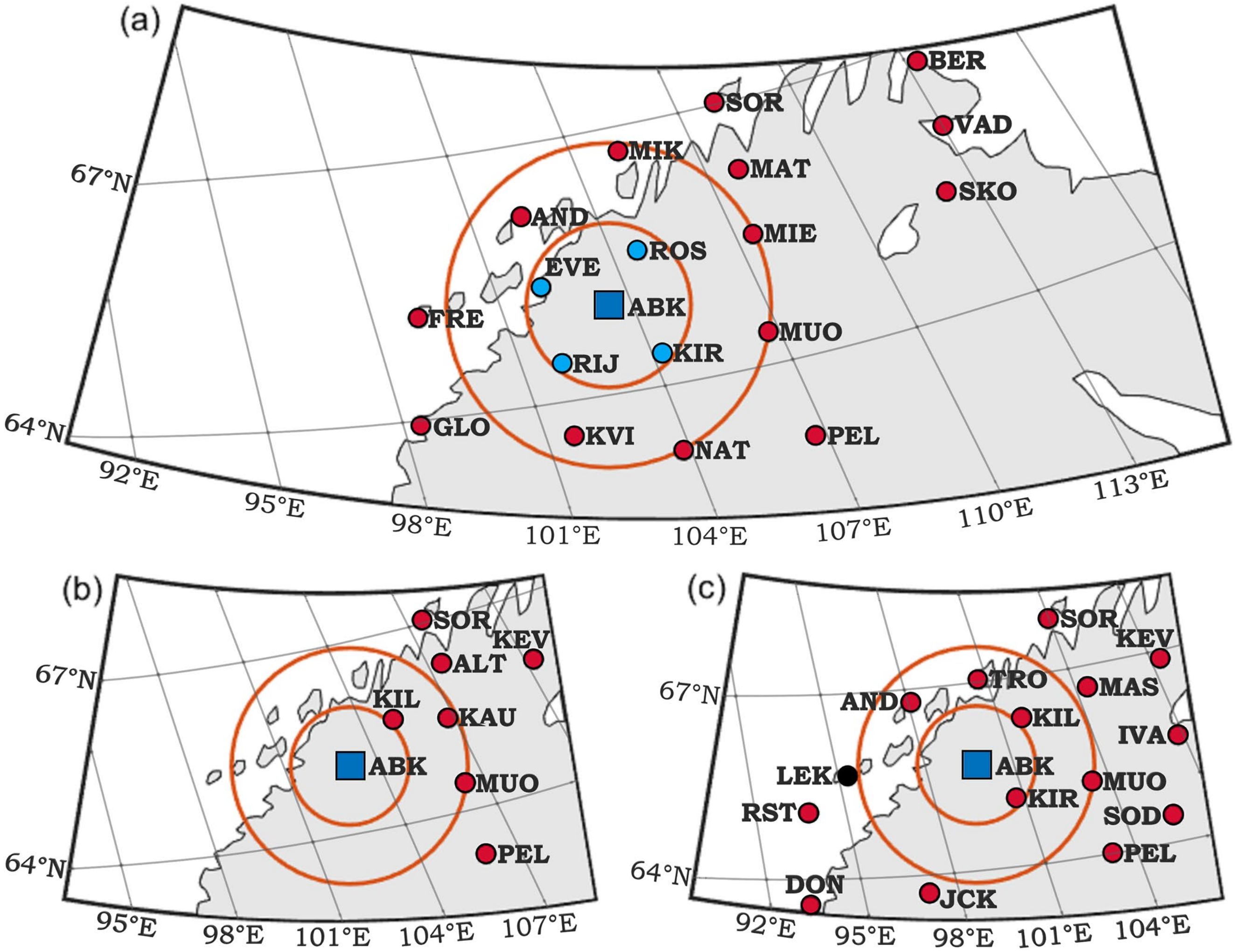

Figure 2. (a) SMA network in CGM coordinates for the year 1977. The red and blue circles show the locations of the SMA stations. The blue square indicates the location of the permanent AE magnetometer station ABK. The inner orange circle shows a distance of 100 km from ABK and the outer 200 km. (b) EISCAT magnetometer cross in CGM coordinates for the year 1983. (c) IMAGE stations in CGM coordinates for the year 2020. The red and black circles show the locations of the IMAGE stations. The AE station ABK joined the IMAGE magnetometer network in 1998. The black-marked LEK station closed in 2005. The CGM coordinates are calculated according to Gustafsson (1970, 1984) and Tsyganenko et al. (1987).

Gough-Reitzel magnetometer. Compared with the original, it was cheaper to manufacture and consumed less energy. The maximum running period increased from 24 days to over 70 days. A normal car battery was replaced with a Dryfit battery, and the location was moved into the tube. The Bulova-Accutron clock was replaced with an electronic quartz-clock, and a timing accuracy increased from ±15 to ±1 s per week on average. Before the SMA field measurements, all instruments were tested and calibrated at the site of the observatory at Wingst of the Deutsches Hydrographisches Institut. The scaling values were changed to fit the conditions in Scandinavia. When the scaling values in Germany were between 10 and 20 nT mm^{-1}, suitable values in Scandinavia were generally 40 nT mm^{-1}. The recording magnets of all instruments were aligned in relation to the magnetic north and vertical direction. After testing and calibration, the movement of the magnets was prevented during transportation to Scandinavia (Küppers & Post, 1981).

The theoretical instrument and component-specific measuring range were mostly determined by the scaling values and the maximum shift of the trace. The measuring range was increased for all the components by creating auxiliary traces recorded on the film when the main trace decreases below or increases above the specified threshold. The auxiliary traces were illuminated with other light sources and mirror splitting (Küppers et al., 1979). The measuring range ends when the auxiliary trace crosses the edge of the film. This occurs during the major

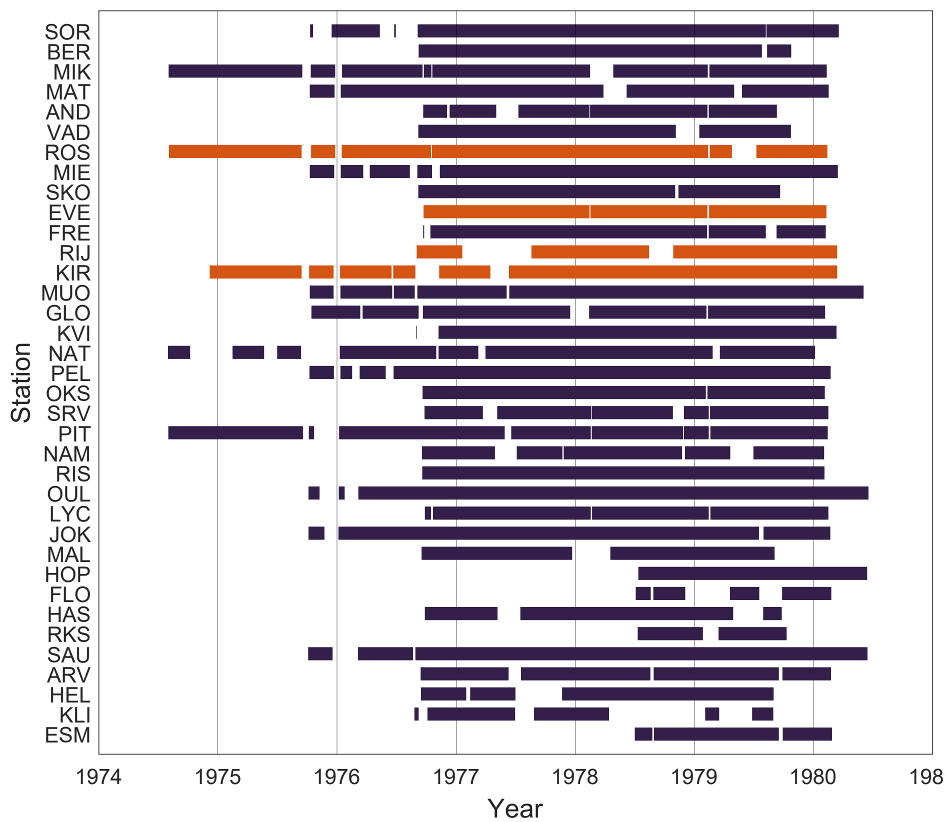

Figure 3. The time intervals for available SMA data. The stations are arranged according to the 1977 CGM latitude. Orange intervals from the stations Rostadalen (ROS), Evenes (EVE), Ritsemjokk (RIJ), and Kiruna (KIR) were recorded around the permanent AE magnetometer station Abisko (ABK).

magnetic storms approximately 20 mm after the main trace has crossed the same edge. The accuracy and capability of the original Gough-Reitzel magnetometers and the SMA instruments have been demonstrated in numerous field operations (Bannister & Gough, 1977; Beer & Gough, 1980; Küppers et al., 1979). The SMA instrument's magnetic resolutions were approximately 2 nT and the magnetic field variations of phenomena lasting more than a minute are well-recorded (Gough & Reitzel, 1967; Küppers et al., 1979).

2.3. SMA Data and DigiMAG Method

The SMA station was buried in the ground to measure unattended for approximately 73 days. After this, the station was prepared for a new measuring interval. The preparation included, among others, the replacement of the battery and camera (Küppers et al., 1979). The last measuring intervals were in 1980, and the total amount of recorded data is approximately 44,000 days and 29 km of Kodak RAR 2498 film. Araki et al. (1992) have sketched a graph that shows the intervals for available data. However, it does not show that there can be a long period of time between the end of the magnetogram and the beginning of a new one. The time intervals with these gaps for available data are shown in Figure 3. The resolution of the graph is 1 day. Thus, a continuous long period indicates that a new measurement interval has started during the same day as the previous one has ended.

Possible instrument failure could not be detected during unattended operation. The total loss of the recordings is approximately 10%, and minor losses are higher (Baumjohann, 1982; Küppers & Post, 1981). The end of the Z-component registration is a common failure in the recordings. Its recording magnet was located near the bottom of the tube and its wire was the longest. Data recorded by the SMA array comprises more than 620 film reels. Sodankylä Geophysical Observatory possess the original recordings. Copies of the recordings were provided to the WDC for Geomagnetism in Kyoto. Each reel has a package with station and time information that makes it possible to find the desired reel.

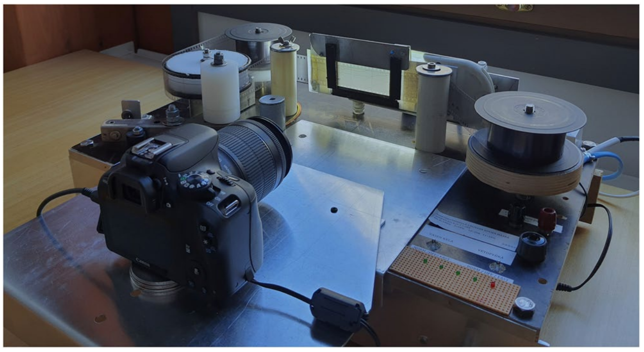

Figure 4. Custom-built digitization device DigiMAG.

The first SMA researchers noticed that its slow optical recording limits the usability of the SMA data (Araki et al., 1992; Küppers et al., 1979). Now decades later, a device, shown in Figure 4, is built for photographing the SMA data. The main motor rotates the film reel, and a camera attached to the device frame takes photos of the film. During one 360° rotation of the main motor shaft, rods attached to the shaft first move the film and trigger the camera. The film is pulled by a wheel with a rubber at the edges to improve friction. The rod attached to the motor shaft pushes the vertical steps at the bottom of the wheel and moves it 30°, or 1/12 of the wheel's circumference, on every round. When the copper rod attached to the main motor shaft goes between the sensor and the LED, an optical switch triggers the camera. The auxiliary motor rotates the photographed film on a blank reel.

Photographing a magnetogram with 73 days of the data takes less than 2 hr. The height of the recorded optical data remains the same in pixels. After the pixel/mm ratio is known, data can be scaled using nT/pixel values. Scaling large amounts of the data with the same usually linearly increasing or decreasing scaling values is possible. This makes data processing less time-consuming. An example of a recording photographed with the digitization device is shown in Figure 5. The main phase of the magnetic storm begins, and the magnetic components H and Z decrease rapidly. The positive amplification direction for these components is downward on the film. Data can be collected from photographs by measuring the trace's distances to the B1 baseline at even intervals. If the trace crosses the film's edge, its theoretical distance can be calculated from the auxiliary trace until the instrument's measuring range ends.

A 3-min resolution of this article is achieved by measuring the values 20 times per hour. The best possible resolution would be 10 s because inside the instrument was a lamp that switched on every 10 s and illuminated the magnet's location in the film (Gough & Reitzel, 1967; Küppers & Post, 1981). The collected data needs to be scaled in order to know the actual variations in the magnetic field. Different film reels have different scaling values for all the components that determine how much one-mm change is in nanoteslas. These scaling values are usually different at the beginning and the end of the film reel. Several film reels also have a positive or negative time delay at the beginning and the end of the film reel. The assumption is that changes in scaling values are linear functions, and delays do not affect the results at 3-min resolution. The delays are less than 2 s in the film reels used in this article.

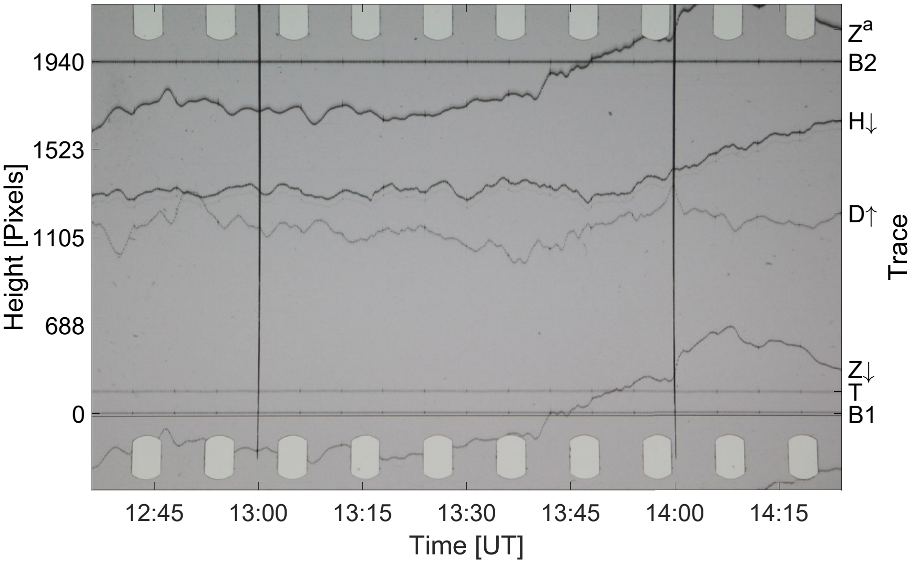

Figure 5. A recording measured at ROS station 27 October 1977. The arrows after the component marks H, D, and Z indicate the direction of the positive amplification of the component. At 13:45, the vertical Z-component decreases rapidly, and the Z^a auxiliary trace rises above the B2 baseline. Usually, on the SMA recordings, the Z-component trace is visible above the B1 baseline, and Z^a auxiliary trace decreases below the B2 baseline only during the strong disturbances.

The collected unscaled data does not show the real variations in the magnetic field. The magnitude of the scaling values varies between and along the recordings. Thus, only a visual inspection of SMA magnetogram is not a reliable method for comparing and examining data. During strong magnetic disturbances, the traces form a lot of intersections. There is a high risk of mixing up the traces if their color and shape match after the intersection. However, due to the different location reflected light rays with respect to the optical axis parallax effect exist which allow identification of the different traces. The recording mirror surfaces of some SMA instruments have been scratched to make the traces of recorded data different looking. The scratches on the mirror stand out as scratches on the recorded trace.

The distance of the trace to the baseline is compared with a quiet time reference (QTR). This reference value is film and component-specific, so it must have occurred during the same film record interval. The film reels examined have been recorded during the following time periods: 19 August 1977 to 02 November 1977 (KIR), 20 August 1977 to 01 November 1977 (RIJ), 22 September 77 to 01 December 1977 (EVE) and 22 September 1977 to 04 December 1977 (ROS). These recording intervals overlap during 22 September 1977 to 01 November 1977 and we have chosen the QTR from this overlapping recording period. The QTR of this paper is 11 October 1977, 07:00 [UT]. The Dst index was 0 nT and very stable for the previous and the next couple of hours. This reference value is measured in pixels from the film reel photos. Then, the value is reduced from each measurement point from the collected data. The value of quiet time is a new x-axis. Then, in the case of H and Z, each data point is multiplied by -1. This turns the image upside down and does not affect any zero points. The image is moved to the correct place in the coordinate axis. After this, each data point is scaled using the calculated nT/pixel value. The data point's scaling value depends on the scaling values at the ends of the film and the distance of the point to these ends. The result of the following function begins to increase or decrease linearly depending on whether the scaling value at the beginning of the film, α, is greater than the value at the end β.

$$f(x) = \alpha - \left(\frac{(\alpha - \beta)(x_n - 1)}{x_{tot}}\right) \tag{1}$$

The number of measurement points, x_{tot}, determines the rate of scaling value change along the measuring points. The measuring point number, x_n, determines the number of the point calculated from the beginning of the film. With a fictional day-long recording and 1-hr resolution, at the measurement point 10:00, $x_{\mathrm{tot}} = 24$ and $x_n = 11$. The first measurement point would be 00:00 and the last one 23:00. If the H-component scaling value is 40 nT at the beginning and 45 nT at the end of the recording, the H-component scaling value is 42,08 nT at 10:00. If the resolution is increased to the 3 min used in this paper, for the same fictional recording at 10:00, $x_{\mathrm{tot}} = 480$ and $x_n = 201$.

Collecting data from the photos is a manual job. The collection benefit/speed ratio is at its best 60 min resolution due to the timestamps of the film. The next best efficiency is at a resolution of 6 min. During the strong disturbances, the traces of the different components intersect, and it takes time to identify traces if the recording mirrors of instruments have not been scratched enough.

2.4. Identification of Storm Period and Space Weather Conditions

During the main phase of the magnetic storm, the Earth's ring current intensifies rapidly and compresses the horizontal component of the surface magnetic field. The disturbance storm time (Dst) index stations are located near the magnetic equator, where the strength of the surface magnetic field is inversely proportional to the energy content of the ring current. As the magnetic field of the interplanetary magnetic field (IMF) turns to point north, the ring current and the Dst begin to recover (Gonzalez et al., 1994; Hamilton et al., 1988; Sugiura, 1964). Thus, the lowest $\mathrm{Dst}_{\mathrm{min}}$ value reached by a magnetic storm depends on its magnitude. When this value is between -50 and -100 nT, a moderate storm is ongoing. A strong storm reaches a value of (-100 nT $\geq \mathrm{Dst}_{\mathrm{min}} \geq -200$ nT). Severe as well as great super-storms reach values below -200 nT (Loewe & Prölss, 1997). Figure 6 shows the magnetic disturbances with the lowest Dst indices of 1977 that were measured when the number of charged particles in the magnetosphere was high. The lowest Dst values of these disturbances are centralized for ease of comparison. During the October event, the Dst decreases to -159 nT, and this period is digitized.

The LRO data is a comprehensively cross-compared near-Earth data source for plasma and magnetic field parameters shown in Figure 6. For 1977, the LRO plasma data sources are IMP-7, IMP-8, and ISEE-1 (Asbridge

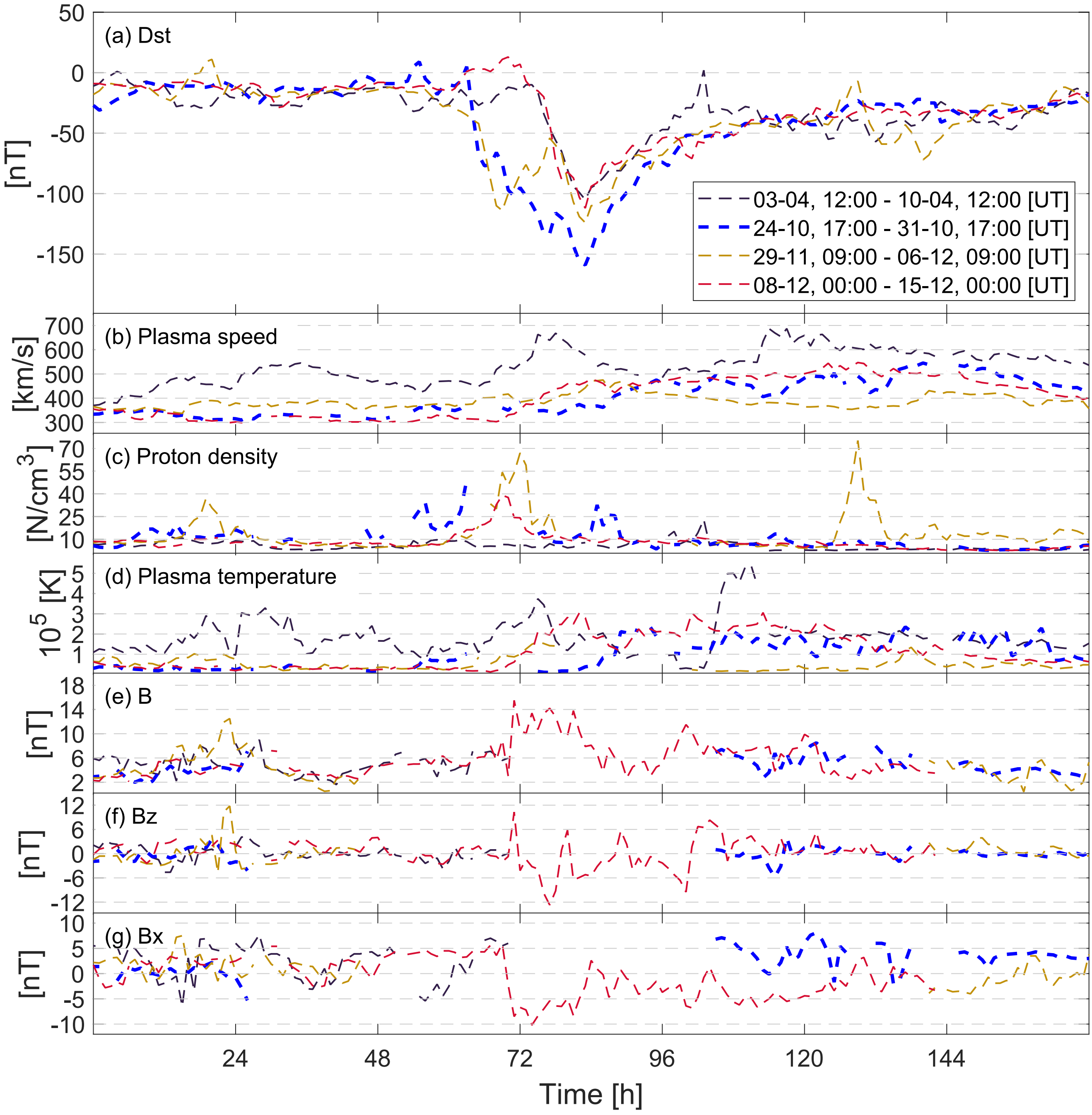

Figure 6. The Dst and low-resolution OMNI (LRO) data. (a) All magnetic disturbances in 1977 with $Dst_{min} \leq -100$ nT. These Dst indices were provided by the WDC for Geomagnetism, Kyoto (Nose et al., 2015b). The index reaches its highest negative value in 1977 during the disturbance period marked in blue. The value was 7 hr continuously lower than the peak value of the disturbance period marked in yellow (b, c, d) SW plasma parameters measured by IMP-7 (Explorer 47), IMP-8 (Explorer 50), and ISEE-1 spacecrafts. (e, f, g) Average scalar field magnitude B, Bz (GSE), and Bx (GSE) measured by IMP 8. The OMNI data were obtained from the GSFC/SPDF OMNIWeb interface at https://omniweb.gsfc.nasa.gov.

et al., 1976; Bame et al., 1978; Lazarus & Paularena, 1998). For the same year, the only LRO near-Earth IMF data source is IMP-8, and it was in the solar wind for 7–8 days during each 12.5 days orbit. Figure 7 shows the orbit during the October event. The spacecraft (SC) reaches the night side of the *x*-axis 25-10, 15:30 and returns on the dayside 30-10, 04:05. The timestamp of the last available parameter after moving on the night side is 25-10, 19:00, and the first one before the dayside 29-10, 02:00.

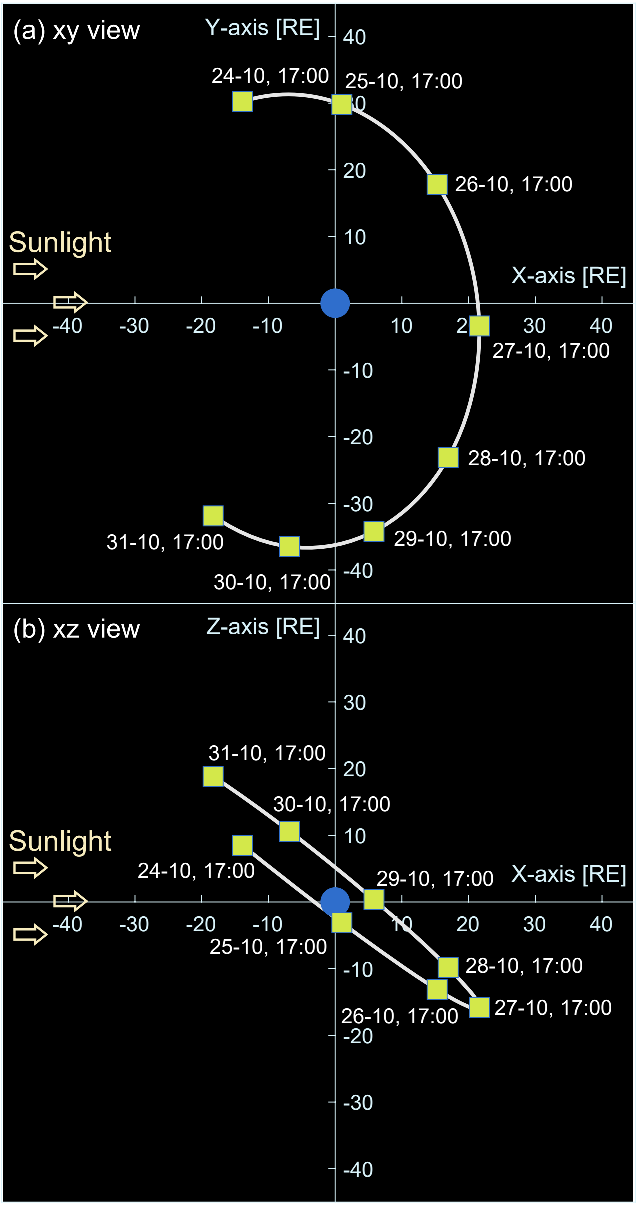

Figure 7. IMP-8 24 October 1977, 17:00 to 31 October 1977, 17:00 orbit (GSE). The position data of the spacecraft were obtained from OMNIWeb.

IMP-7 was on the dayside until 28-10, 13:48, and the LRO data contain plasma parameters recorded by it between 25-10, 21:00 and 29-10, 01:00. Its payload included instruments for recording IMF parameters, but the data time span ended in 1973. ISEE-1 SC was launched 22 October 1977 and the available plasma data begins 30 October 1977 (Asbridge et al., 1976; Bame et al., 1978; Lazarus & Paularena, 1998).

There is a correlation between the emergence of geomagnetic storms and the occurrence of coronal mass ejections (CMEs) (Burlaga et al., 1981; Wilson & Hildner, 1984). In order to cause a strong geomagnetic storm, the corona must erupt toward Earth and be accompanied by a southward magnetic field component (Gonzalez et al., 1994; Russell et al., 1974).

The Earth's magnetosphere internal rotation movement enhances as the IMF carries a negative Bz component to the magnetopause. The Earth's magnetic field is pointing in the opposite direction and tears open under the flow of the IMF. With a phenomenon known as magnetic reconnection, the IMF field lines connect to these open Earth field lines (Dungey, 1953, 1961). The combined field lines travel within the solar wind to the night side of the Earth and accumulate magnetic flux in the tail lobes. Part of this energy is discharging within the returning field lines into the polar ionosphere (Aubry & McPherron, 1971).

Occasionally, the solar wind carries large structures with different magnetic characteristics compared with the ambient environment. These magnetic clouds (MC) are defined as the areas in the solar wind where the magnetic field has enhanced strength, the direction of the measured field changes smoothly when an SC passes through the MC and proton temperature (and beta) are low in comparison with the ambient values (Burlaga, 1988; Burlaga et al., 1981). The solar wind magnetic field parameters are needed for comprehensive multimethod SMA data analysis.

The resolution of IMP-8 magnetic data is 320 ms, and data is recorded regardless of the orbit phase. This article uses a 1-min average data set created by NASA's SPDF in 2009. One-minute averages were calculated using a 15.36 s magnetic field data set. The data period is mainly flagged, meaning that the data is not from the solar wind, and critical interpretation is emphasized. Figure 8 shows the Dst and the best available space-borne data for the October event. The magnetic equator is under the impact of the greatest magnetic storm of 1977. For the SMA network located at a higher latitude, the storm period is divided into three major substorms based on the digitized data.

Plasma speed and proton temperature are relatively low and rise slightly as the ring current begins to recover. Proton density increases as the Dst begins to decrease. Thus, it seems the Bz orientation has not changed during the passage to the magnetosphere, and IMF feeds the magnetosphere with the new particles when the night side Bz is negative. The magnetic field strength (B) rises sharply on the night side and reaches its peak as the SC passes through the magnetotail. The stretched magnetotail can be seen as a low Bz value when IMP-8 is around the maximum distance on the x-axis on the night side.

3. Results

The clearest average characteristic of a magnetic storm is the rapid decrease of the H-component and its subsequent slow recovery (Chapman & Bartels, 1940). This decrease is the consequence of an increase in the number of particles trapped in the magnetosphere. The ring current is formed by ions and electrons moving in different directions from midnight. Ions are moving toward dusk and electrons toward dawn. The H-component decrease

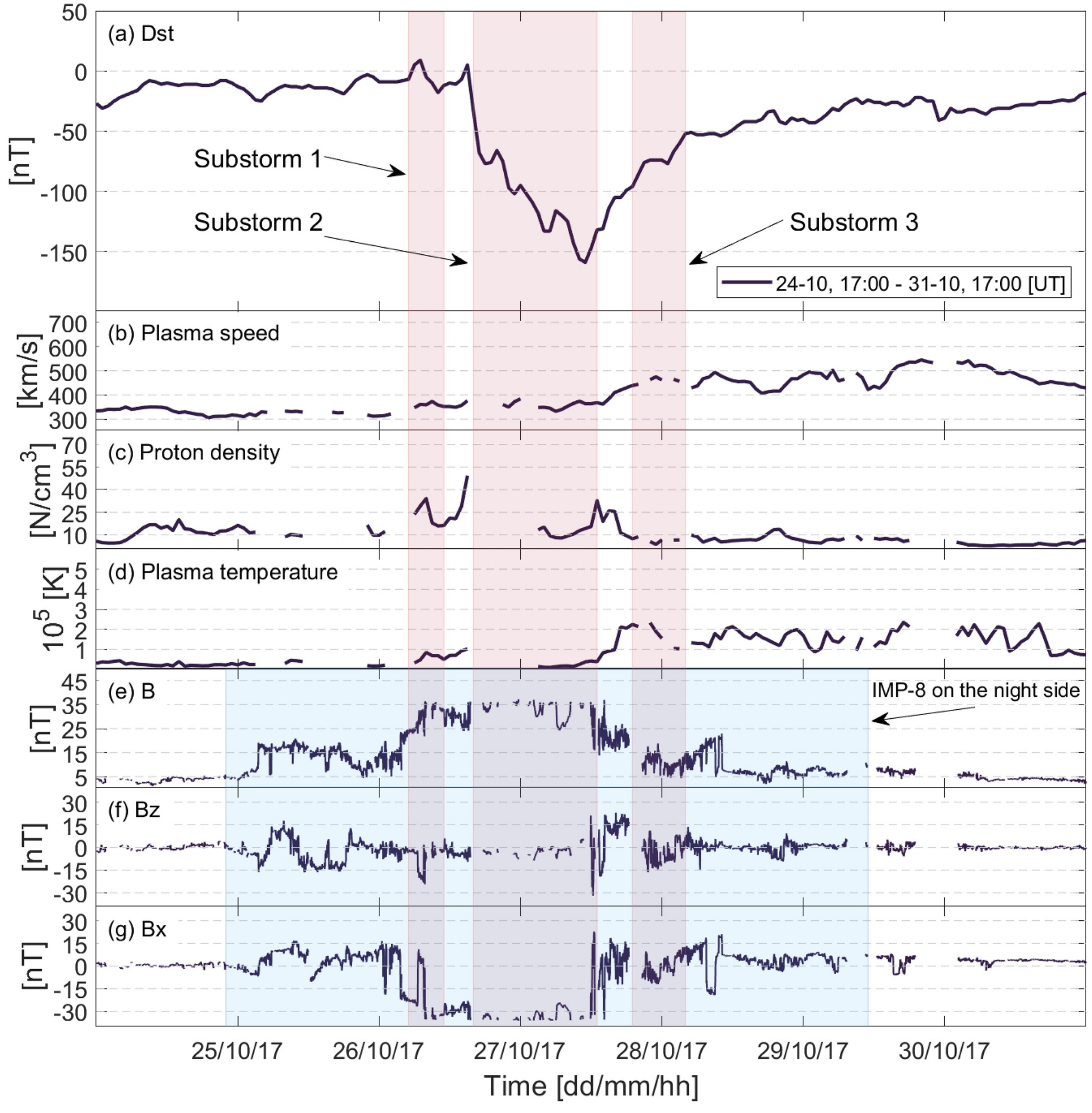

Figure 8. The Dst, LRO plasma parameters, and merged IMP-8 1-min data. The vertical columns divide the storm period into three substorms and the horizontal box shows when IMP-8 is on the night side of the Earth in GSE coordinates. (a) Dst index. (b, c, d) LRO plasma parameters. (e, f, g) SPDF 1-min average magnetic field parameters Scalar B, Bz (GSE), and Bx (GSE).

lasts for several hours or even days when the southward interplanetary magnetic field (IMF) feeds the magnetosphere with the new particles (Gonzalez et al., 1994). It is recognized that the ring current is asymmetric during the main phase of the magnetic storm. Furthermore, this dawn-dusk asymmetry causes substantially stronger magnetic disturbances on the dusk side (Fok et al., 1996; Grafe, 1999; Walsh et al., 2014). The effects of the magnetic storm on the equator are seen as substorms at the high latitude. These substorms appear as strong fluctuations in the H-component shown in Figure 9. The right side *y*-axis of the Dst index indicates the similarity in the horizontal magnetic disturbances at a magnetic equator and high latitudes.

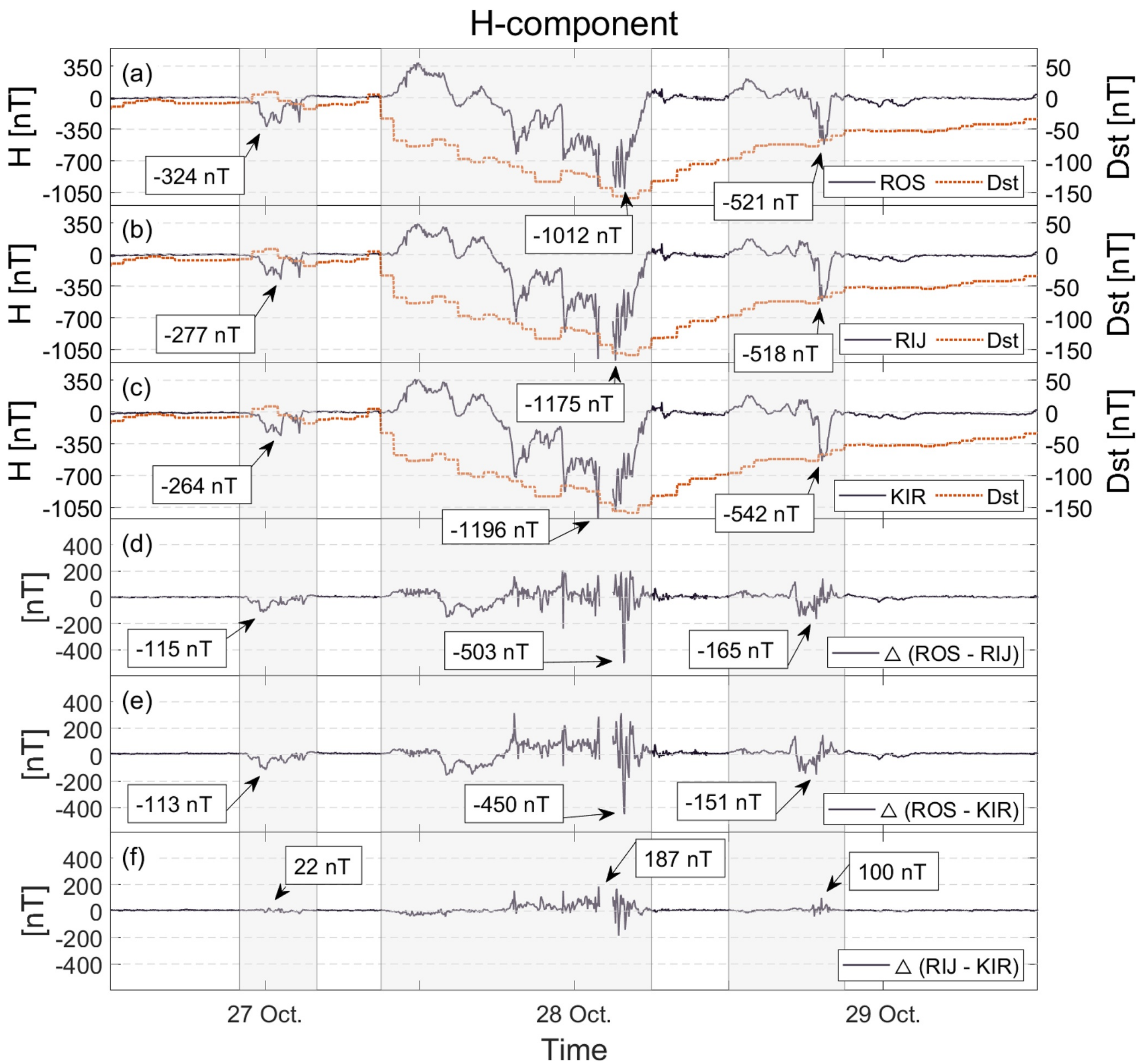

Figure 9. The Dst index marked in orange and digitized H-components of (a) Rostadalen (ROS), (b) Ritsemjokk (RIJ), and (c) Kiruna (KIR). The storm-time data 28 October 1977, 02:00–03:00 UT was too intense to be digitized. The difference of ROS and RIJ (d), ROS and KIR (e), and RIJ and KIR (f) are shown with the same *y*-axis scaling.

3.1. Digitized H, Z, and D Components

The three largest substorms have been identified from the storm of 26–30 October 1977. This separation is made according to the lowest resolution (LRO) 1 hr data to allow multimethod data analysis and is shown in Figures 9–15 with light gray shading. The beginning and ending of the substorms are given in Table 2.

Subtracting the data from lower latitude stations from the higher latitude data indicates the high momentary differences over a short magnetic north-south distance. The largest difference occurs during the recovery phase of substorm 2. The west-east differences are minor in comparison with the above-mentioned. Substorm number 1 occurs with a peak amplitude of −324 nT (ROS) during the initial phase of a magnetic storm. The Dst measured at the equator increases, and the H-component measured by the SMA network's stations studied decreases. The second substorm begins at 09:18 in ROS, at 09:57 in RIJ and KIR, simultaneously to the beginning of the storm

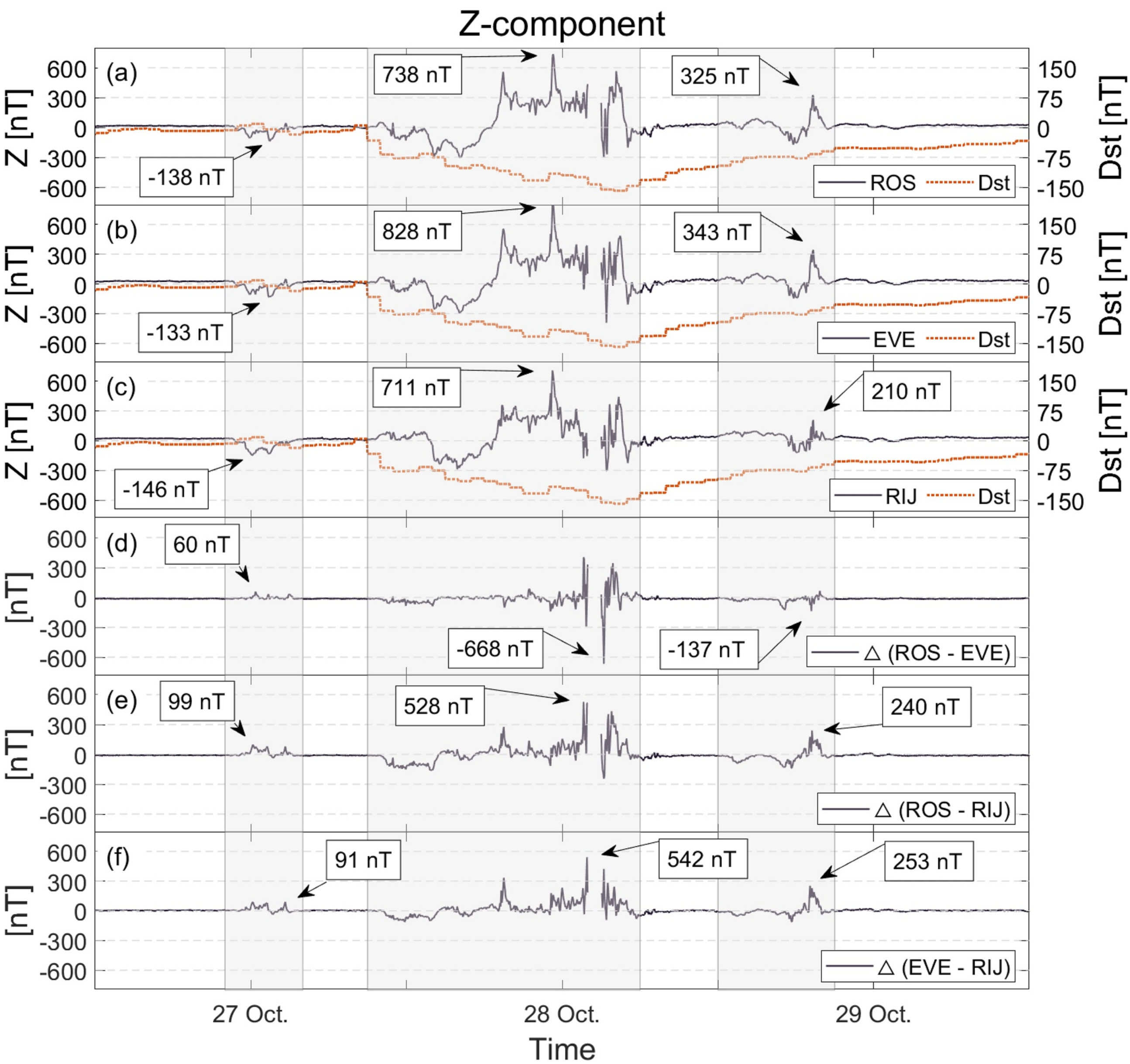

Figure 10. (a, b, c) Digitized Z-component traces and the Dst index. The Z-component of KIR station could not be digitized due to missing component trace registration. The difference curves are shown for (d) ROS and EVE, (e) ROS and RIJ, (f) EVE and RIJ.

main phase and reaches its maximum amplitude −1,196 nT (KIR) on October 28 at 01:51 during the expansion phase. Then, SMA network is on the dawn side. The Dst reaches its lowest value −159 nT at 04 UT.

The third substorm starts exactly at the same time in all three stations, but it ends at 20:15 in KIR, and 3 and 18 min earlier in RIJ and ROS, respectively. The second substorm was longest lasting 20hr 21 min, while the first substorm last 4 hr 30 min and the third 8 hr 15 min. While momentary differences of ROS station to the lower latitude stations remains mainly within 200 nT, at the interface between the end of the expansion phase and the beginning of the recovery phase, occurs −503 nT (ROS-RIJ) and −450 nT (ROS-KIR) differences between these stations. The largest difference between approximately the same latitude stations (RIJ-KIR) is −183 nT.

The subtraction images indicate the average differences between the stations in the vertical magnetic disturbances are smaller in the magnetic east-west direction than the magnetic northeast-southwest and the magnetic north-south directions. After the recovery phase at the equator has begun, the digitized main substorm reaches the level

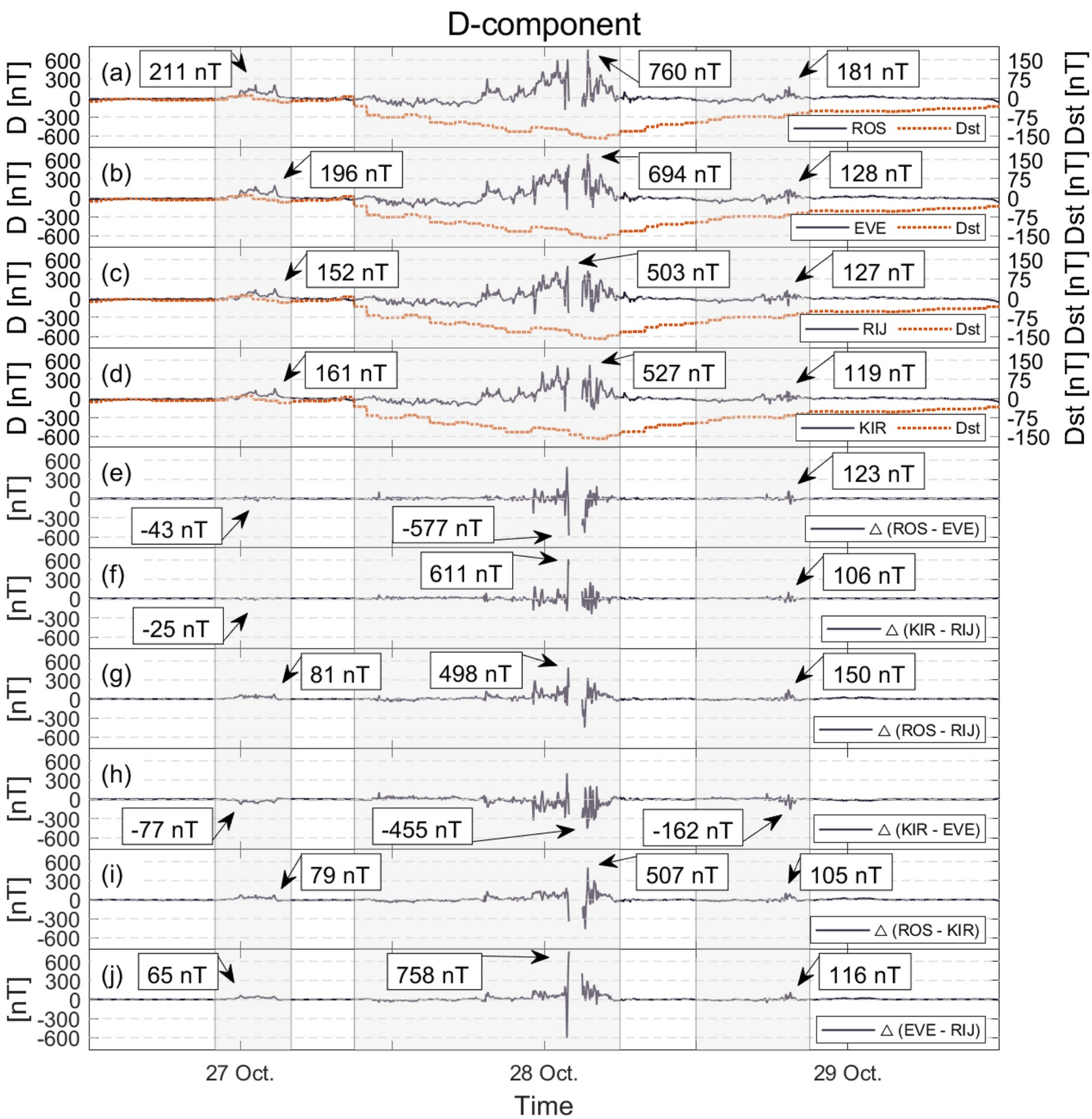

Figure 11. (a, b, c, d) Digitized D-component for ROS, EVE, RIJ, and KIR together with the Dst. The difference curves are shown for (e) ROS and EVE, (f) KIR and RIJ, (g) ROS and RIJ, (h) KIR and EVE, (i) ROS and KIR, and (j) EVE and RIJ.

of quiet time for the first time at 05:39 ROS and RIJ stations. KIR station, located 1.20 CGM latitude degrees below ROS station and 0.08° below RIJ station, reaches this level at the next measurement point 3 min later. Thus, all the three SMA stations have reached quiet time level approximately 3.5 hr after the expansion phase of the strongest substorm reaches its peak. This occurs at the interface of dawn just before sunrise.

The Z-component variation is smaller than in the H-component and the strength increase occurs in the opposite direction (Chapman & Bartels, 1940). While the largest values of the Z-component are −146 nT (RIJ) for substorm 1, 828 nT (EVE) for substorm 2, and 343 nT (EVE) for substorm 3, corresponding peak values of the H-component are −324 nT (ROS), −1,196 nT (KIR), and −542 nT (KIR). Figure 10 shows the Z-component's rapid growth during the expansion phases of substorms 2 and 3.

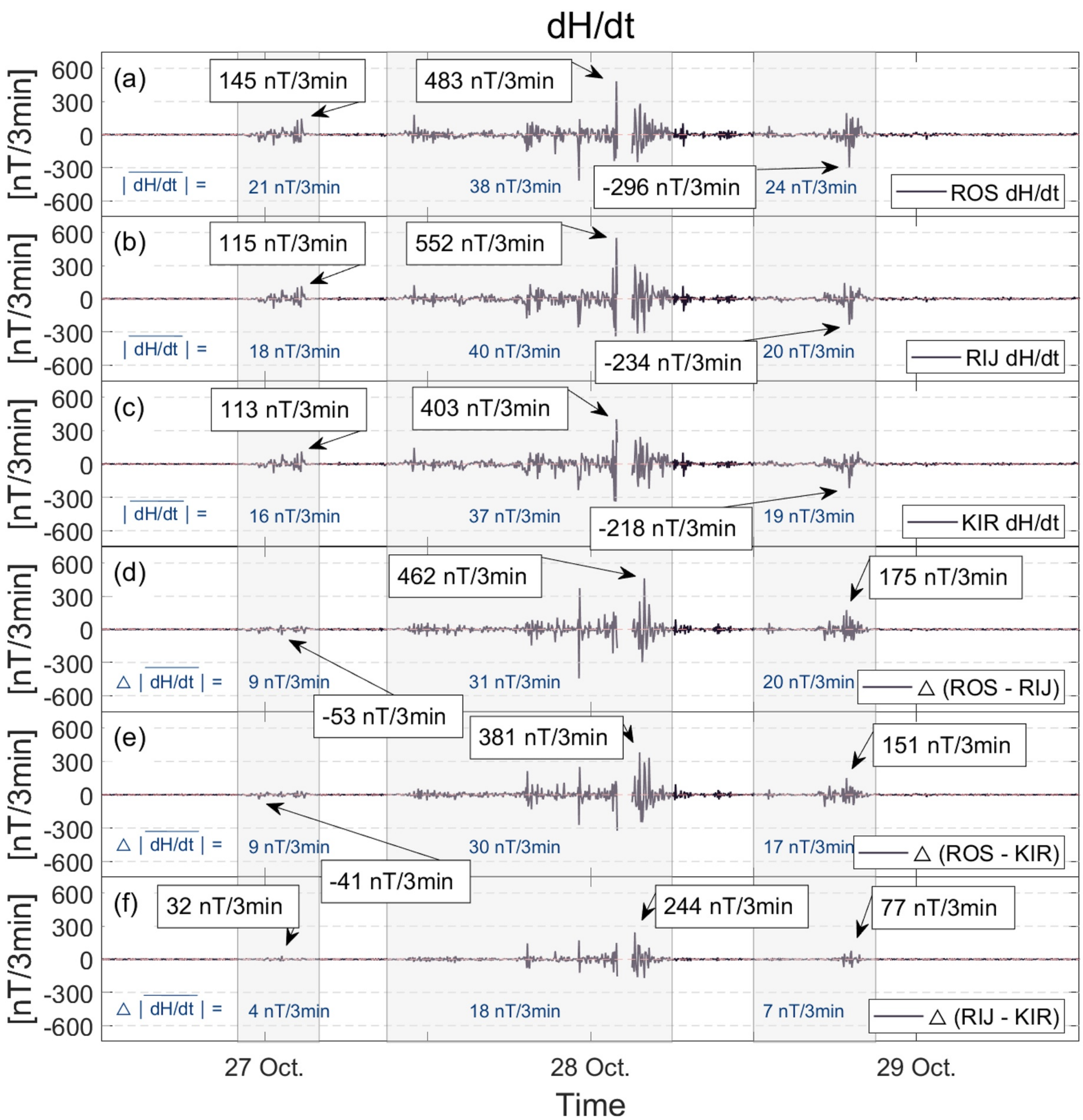

Figure 12. Time derivatives of H-component from 3 min resolution data for (a) ROS, (b) RIJ, and (c) KIR. The difference curves between these three stations are shown in panels (d), (e), and (f). The absolute average time derivatives $|\overline{dH/dt}|$ are shown in the lower left corner of each panel. The average absolute differences between the time derivatives of the stations are denoted $\triangle|\overline{dH/dt}|$.

During the expansion phases of the substorms, the Z-component reaches the highest positive values at approximately the same time as the H-component reaches the lowest negative values. These extremes are manifested as momentary strong changes in the H- and Z-traces in the digitized SMA data.

As shown in Figure 11, in the vicinity of 65° latitude, at ROS, EVE, KIR, and RIJ stations, strong disturbances occur in the D-component simultaneously with the variations in the ring current strength measured by the Dst.

The D-component increases to values 760 nT (ROS), 694 nT (EVE), 503 nT (RIJ), and 527 nT (KIR) during the second substorm. While the largest values of the first substorm are 211 nT (ROS), 196 nT (EVE), 152 nT (RIJ), and 161 nT (KIR). During the third substorm identified from the storm period, the D-component increases to values 181 nT (ROS), 128 nT (EVE), 127 nT (RIJ), and 119 nT (KIR).

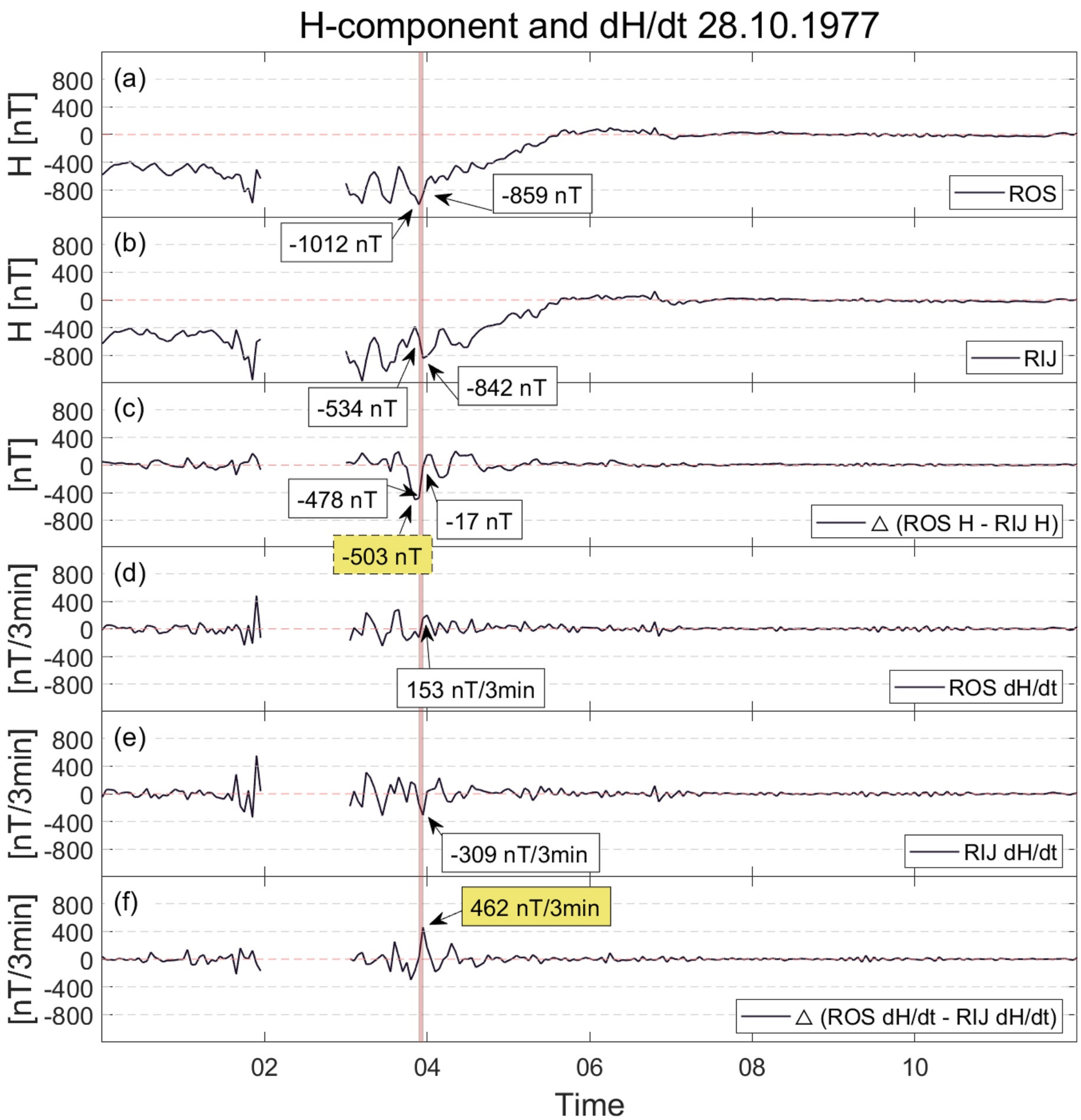

Figure 13. Digitized H-components of (a) Rostadalen (ROS), (b) Ritsemjokk (RIJ). The difference of ROS and RIJ is shown in panel (c). Time derivatives of H-component from 3 min resolution data for (d) ROS, (e) RIJ. The difference in time derivatives of ROS and RIJ stations is shown in panel (f).

The subtraction images indicate that the highest average difference between the stations in the eastern magnetic disturbances occurs between the southeast-northwest direction (KIR-EVE). This average difference is 35 nT for all three identified substorms and 47 nT for substorm 2. The average differences of the other D-component subtraction images range between 20 and 30 nT for all three substorms and 30–39 nT for substorm 2. The following differences arise between stations during the expansion Phase 758 nT (EVE-RIJ), 611 nT (KIR-RIJ), −577 nT (ROS-EVE), and 498 nT (ROS-RIJ). The largest differences in the north-south direction arise at the interface between the end of the expansion phase and the beginning of the recovery phase and they are 507 nT (ROS-KIR) and −455 nT (KIR-EVE).

3.2. Derivatives

Figure 12 shows time derivatives for the H-component. When $t = 6$ min, the substorm is considered having begun when SMA station's $|dH/dt| > 10$ nT and H-component trace increases in the direction of the derivative without

10.1029/2022JA030311

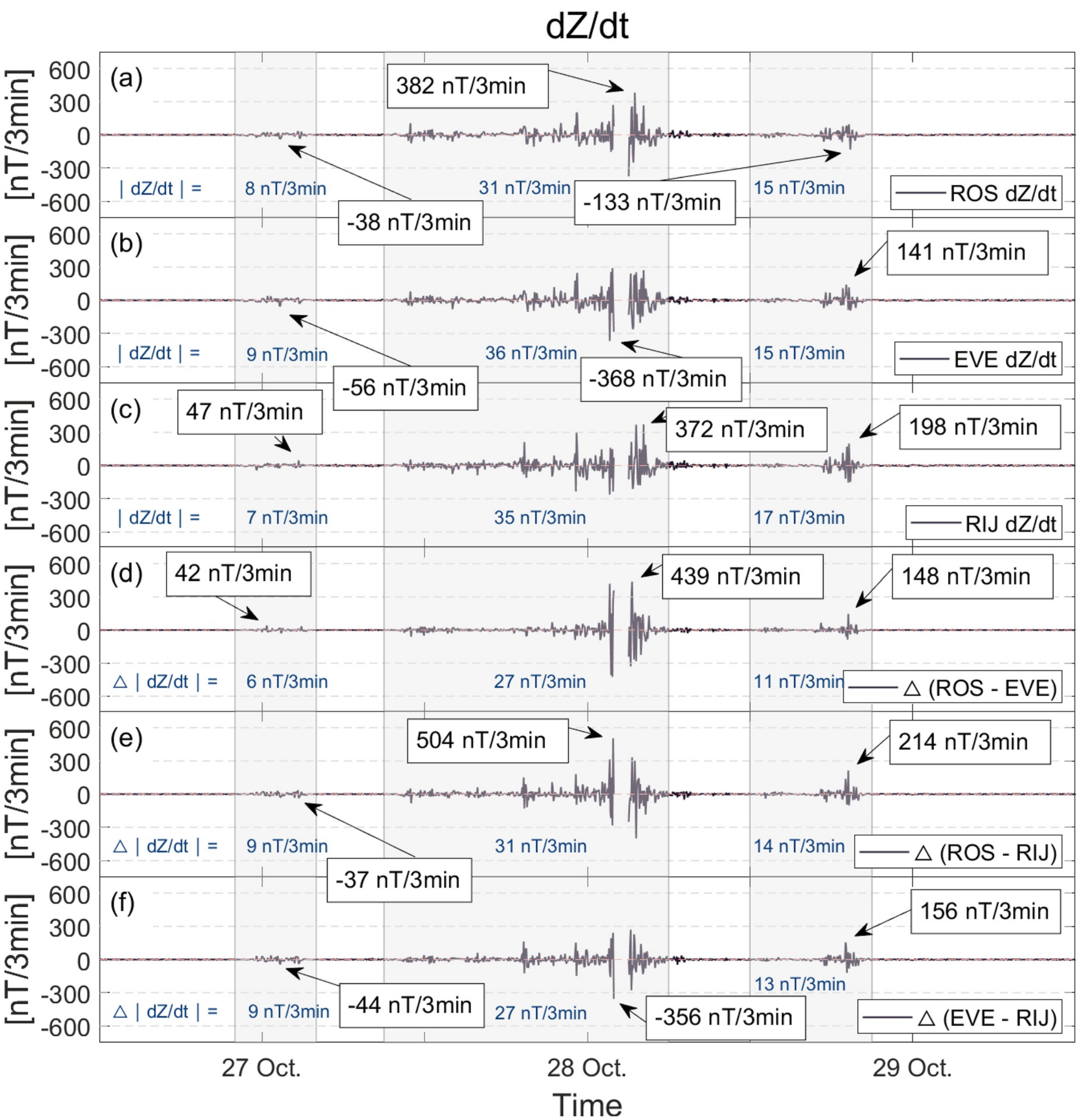

Figure 14. Time derivatives of Z-component from 3 min resolution data for (a) ROS, (b) EVE, and (c) RIJ. The difference curves between these three stations are shown in panels (d), (e), and (f). The absolute average time derivatives $|\overline{dZ/dt}|$ are shown in the lower left corner of each panel. The average absolute differences between the time derivatives of the stations are denoted $\triangle|\overline{dZ/dt}|$.

returning to the QTR threshold. This threshold determines the point on the magnetogram to which the change is compared and is described in Section 2.3. The recovery phase ends when the H-component reaches the QTR value for the first time after the substorm-specific peak amplitude H_{min} show in Table 2.

Changes in the space weather cause geomagnetically induced currents (GICs) at the ground level. The Earth's conductive land structure acts as a conductor of GIC (D. J. Thomson & Weaver, 1975). Part of these currents are grounded in power networks. The greatest GICs are strongly associated with large changes in dH/dt value (Viljanen et al., 2001). A case is known where the dH/dt value reached roughly 10 nT/s at Eskdalemuir Observatory and GIC measuring instrument, located almost 100 km away, measured a peak value of 42 A (A). The "risk limit" for a GIC that damages power systems is considered to be 25 A (A. W. P. Thomson et al., 2005; Freeman et al., 2019).

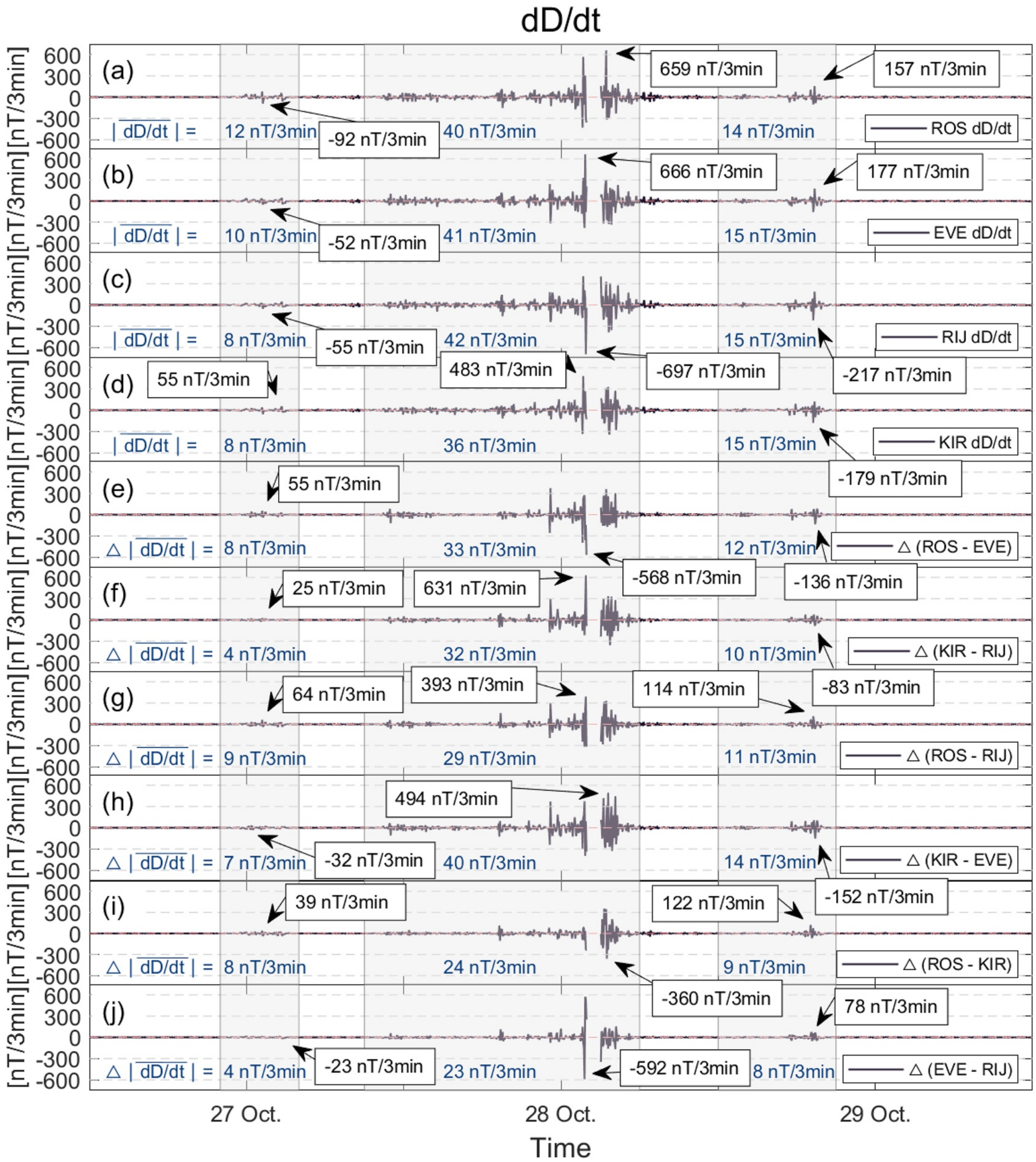

Figure 15. Time derivatives of D-component from 3 min resolution data for (a) ROS, (b) EVE, (c) RIJ, and (d) KIR. The difference curves between these three stations are shown in panels (d), (e), (f), (g), (h), (i), and (j). The eastern component has the largest effective range, $697\ \text{nT} \leq |dD/dt|$.

During the recovery phase of the second substorm, 2.8 nT km^{-1} difference arise between the ROS and RIJ in 3 min. The formation of this difference is shown in more detail in Figure 13. As shown in Figures 13a and 13b, 28 October 1977, 03:54, the H-component is −1,012 nT at ROS station and −534 nT at RIJ station. Three minutes later at the next measuring point, 03:57, these values are ROS −859 nT and RIJ −842 nT. The time derivatives of the stations, shown in Figures 13d and 13e, are ROS 153 nT/3 min and RIJ −309 nT/3 min. Thus, in 3 minutes, 462 nT/3 min difference arise in the H-component time derivatives between Rostadalen (ROS) and Ritsemjokk (RIJ) SMA stations which are located 167 km from each other. The largest momentary difference between the H-component of studied SMA stations, −503 nT, occurs 03:51 and is dash lined in Figure 13c.

Figures 12a, 12b and 12c show that latitude affects horizontal storm-time absolute average time derivatives that are denoted $|\overline{dH/dt}|$. Excluding during substorm 2 at ROS and RIJ stations, these average derivatives are larger at higher latitudes. When we digitize long measurements periods and consider the effect of latitude, it can

Table 2
Start and End Times of the Substorms (UT)

Station	Substorm 1		Substorm 2		Substorm 3	
	Start	End	Start	End	Start	End
ROS	26-10, 22:39	27-10, 03:09	27-10, 09:18	28-10, 05:39	28-10, 12:00	28-10, 19:57
RIJ	26-10, 22:48	27-10, 02:54	27-10, 09:57	28-10, 05:39	28-10, 12:00	28-10, 20:12
KIR	26-10, 22:51	27-10, 02:54	27-10, 09:57	28-10, 05:42	28-10, 12:00	28-10, 20:15
	Δt	H_{min}	Δt	H_{min}	Δt	H_{min}
ROS	4 hr 30 min	−324 nT	20 hr 21 min	−1,012 nT	7 hr 57 min	−521 nT
RIJ	4 hr 6 min	−277 nT	19 hr 42 min	−1,175 nT	8 hr 12 min	−518 nT
KIR	4 hr 3 min	−264 nT	19 hr 45 min	−1,196 nT	8 hr 15 min	−542 nT

Note. Start and end times could not be defined for EVE station due to missing H-component trace registration.

be assumed that this ratio is higher near the SMA stations studied than at the northernmost stations in the vicinity of 67° CGM latitude.

The ratio between the average positive and negative time derivatives of the magnetic field's horizontal component is named a positive derivative negative derivative (PdNd). It answers whether the H-component tends to change more rapidly in the positive or negative direction. The PdNd value can be computed by the following equations

$$Pd = \overline{dH/dt}, \quad when \quad dH/dt > 0 \tag{2}$$

$$Nd = \overline{dH/dt}, \quad when \quad dH/dt < 0 \tag{3}$$

$$PdNd = |Pd/Nd| \tag{4}$$

The PdNd makes it possible to compare the dynamics of substorm between stations and between different substorm phases. If the value is less than 1, the expansion phase has had a stronger effect on the H-component than the recovery phase (and possible growth phase). The Pd and Nd numbers are calculated from the beginning of the substorm to the end of the recovery phase. For the substorm 2, the PdNd values are ROS 1.05, RIJ 1.02, and KIR 1.03. The growth and recovery phase has stronger effect to the H-component at higher latitude (ROS) than the lower latitudes (RIJ) and (KIR).

Substorm 1 and its time derivatives are small in comparison with other identified substorms. The maximum values for the H-component are 145 nT/3 min (ROS), 115 nT/3 min (RIJ), and 113 nT/3 min (KIR). While the corresponding values for the Z-component, shown in Figure 14, are −38 nT/3 min (ROS), −56 nT/3 min (EVE), and 47 nT/3 min (RIJ).

When considering all the three substorms, the strongest rapid changes in the magnetic field occur at the end of the expansion phases and the beginning of the recovery phases. The data in the magnetograms is unreadable 28 October 1977, 02:00–03:00. This part of the recording from ROS station will be shown in the discussion. The measuring range ends before the theoretical ability to record strong disturbances. Küppers et al. (1979) estimated that the total measuring range for a typical instrument is from −1,500 nT to +1,000 nT for H-component, from −500 to +1,000 nT for D-component and from −800 to +1,200 nT for Z-component. These values roughly correspond to the boundary where the auxiliary trace crosses the edge of the magnetogram. Recorded data is not always readable although the auxiliary trace, described in Section 2.2, does not exceed the edge of the magnetogram. When there were rapid and strong changes in the magnetic field, the instrument did not have time to record the rapid and wide movement of the magnets on the film properly. Thus, we determine effective measuring range by using the largest time derivatives of the components studied and when $t = 3$ min, this range is 552 nT $\leq |dH/dt|$, 697 nT $\leq |dD/dt|$, and 382 nT $\leq |dZ/dt|$ compared to the QTR, described in Section 2.3.

Despite an effective measuring range, the difference between the component time derivatives can be higher when the derivatives of the stations increase in different directions. As shown in Figure 14e, the largest difference between the Z-component time derivatives is 504 nT/3 min.

During the expansion phase of the substorm 2, in 3 min, 3 nT km^{-1} difference arise between the vertical Z-component time derivatives of ROS and RIJ stations. Plasma speed and proton density, shown in Figure 8, have increased before substorm 3. These plasma properties and the associated magnetic fluctuations can be thought of as causing substorm 3. This substorm is more dynamic and causes large differences in the north-south direction. During this substorm, the largest derivatives of the stations for the H-component are −296 nT/3 min (ROS), −234 nT/3 min (RIJ), and −218 nT/3 min (KIR). While the corresponding values for the Z-component, shown in Figure 14, are −133 nT/3 min (ROS), 141 nT/3 min (EVE), and 198 nT/3 min (RIJ). As shown in Figure 15, the largest D-component time derivatives of the stations for the substorm 3 are 157 nT/3 min (ROS), 177 nT/3 min (EVE), −217 nT/3 min (RIJ), and −179 nT/3 min (KIR).

During the substorm 2, a difference of 5.1 nT km^{-1} occurs between the D-component time derivatives of KIR and RIJ stations. The distance between these stations is 124 km. During this substorm, the D-component has a higher absolute average time derivatives (40 nT/3 min [ROS], 41 nT/3 min [EVE], 42 nT/3 min [RIJ], and 36 nT/3 min [KIR]) than the H-component (38 nT/3 min [ROS], 40 nT/3 min [RIJ], and 37 nT/3 min [KIR]), and Z-component (31 nT/3 min [ROS], 36 nT/3 min [EVE], and 35 nT/3 min [RIJ]). With the exception of KIR station, where horizontal absolute average derivatives reach 37 nT/3 min, the strongest average changes in the magnetic field occur in the east-west component during the substorm 2. These strongest average changes occur in the horizontal H-component at all the stations during the substorms 1 and 3.

4. Discussion

We analyze the newly digitized SMA network data, which was recovered by using a DigiMAG method. Data usability has long been limited by time-consuming optical recording and difficult digitization mentioned by Küppers et al. (1979) and Araki et al. (1992). A custom-built device and DigiMAG method developed allows data to be recovered efficiently. The largest storm of the year 1977 was selected to be digitized.

The AE index is available at WDC for Geomagnetism at Kyoto (Nose et al., 2015a). The AE index for 1976 (January–April), 1977 (January–December), 1988 (July–December), and 1989 (January–February and April–December) have not yet been derived. There is an urgent need to rescue old data. Old data have benefited space weather studies even for the recent events (Hayakawa et al., 2021; Knipp et al., 2016). Space weather activity has been measured in the Scandinavian region for a long time (Hayakawa et al., 2019; Nevalinna, 2006).

When a value of $Dst_{min} = -159$ nT is measured at the equator, a magnetic storm is classified as strong (Loewe & Prölss, 1997). Storm-time recordings were digitized from four SMA stations: Rostadalen (ROS), Evenes (EVE), Ritsemjokk (RIJ), and Kiruna (KIR). As a permanent magnetometer station, Abisko (ABK) is an important data source for geophysical research. It is located on the edge of the auroral zone during moderately active times, and in this study we studied how the magnetic field changes in its vicinity. Advanced artificial intelligence (AI) could convert photographic data into numerical form. More than half of the data does not contain intersections and is thus digitizable with this method. Over 22,000 days of data could be read without solving this challenge. Together with DigiMAG, this would satisfy the need for automatic digitization proposed by Araki et al. (1992) and would allow for statistical analysis mentioned by Küppers et al. (1979). More advanced AI methods would be needed for digitizing the data with intersections.

Our results show strong and localized disturbances in the magnetic field in the vicinity of the 65° latitude during the magnetic storm on 24–31 October 1977. The changes in the horizontal component occur almost simultaneously with the changes in the Dst index. The horizontal differences reach more than 500 nT over a distance of 167 km. This indicates that a dense network of magnetometers would be needed to measure rapid localized changes and to study geomagnetic activity close to the auroral oval. The highest values are measured when the measurement capacity of SMA instruments has been at its maximum. Individual station data near the data gap should be viewed critically. A comparison of the digitized data to the permanent magnetometer data shows that the digitization of the storm period has been successful overall. Compared to the QTR threshold 11 October 1977, 07:00, the point on the magnetogram to which the change is compared, the lowest digitized H-component of the stations were ROS −1,012 nT, RIJ −1,175 nT, and KIR −1,196 nT. Most likely, the H-component decreases even lower values at all stations during the data gap on October 28, 02:00–03:00. In the IMAGE magnetometer network area, the mean IL intensity of storm-time substorms during years 1997 and 1999 was −665 nT (E. I. Tanskanen et al., 2002).

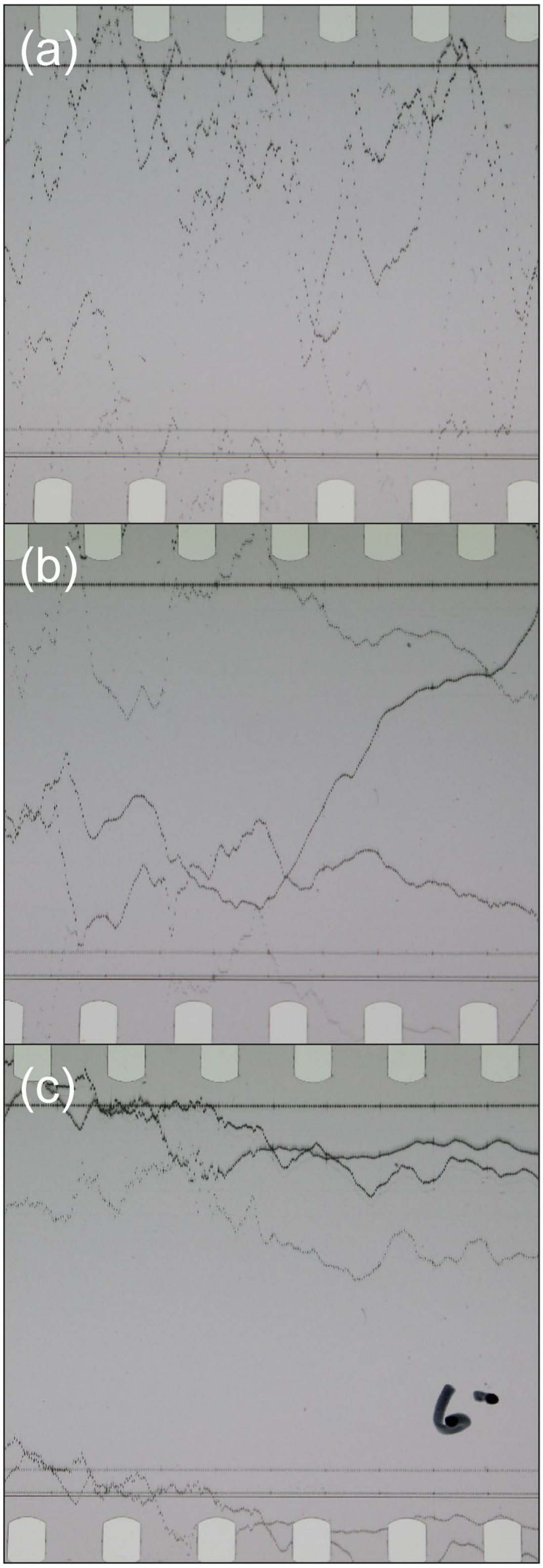

Figure 16. Recordings from ROS station measured on 28 October 1977. (a) 02:00–03:00, (b) 04:00–05:00, (c) 05:00–06:00.

In 3 min, 2.8 nT km^{-1} difference arose in H-component time derivatives between Rostadalen (ROS) and Ritsemjokk (RIJ) stations. The distance between ROS and RIJ stations was 167 km. Identified substorms are strong and large derivatives occur in all three components of the magnetic field. Applications such as navigation, aviation, energy supply, and telecommunications need information on the magnetic field strength. Our results show that the direction of the change in the intensity of the magnetic field can be very different over a short distance. The PdNd method enables comparison of rapid magnetic field changes during substorm phases. During substorm 2 studied, the growth and recovery phase has stronger effect to the H-component at higher latitude station Rostadalen (ROS), than the lower latitude stations Ritsemjokk (RIJ) and Kiruna (KIR).

Figure 16a shows the time interval when the measuring range of the type Münster Gough-Reitzel magnetometer was exceeded. The instrument recorded small fluctuations during the recovery phase. These appears as small spikes in the trace registration and shown in Figure 16c. Due to missing component trace registration, the H-component of EVE station could not be digitized. When the two missing component trace registrations and the exceeding of the instrument's measuring capacity are removed, the amount of valid data for the examined period is 82%. We were able to collect valid data values from SMA magnetograms using the DigiMAG method. Figure 17 shows the comparison of the digitized data and the data measured at ABK station. Consistency indicates that digitization has been successful.

5. Conclusions

1. DigiMAG method works. It was developed for digitizing magnetic data from the 35 mm film as used by the SMA magnetogram systems. The film reels are becoming obsolete and there is an urge to save the valuable data. The year 1977 is the only full year for which an AE index has not been produced since 1957.
2. Differences in the magnetic field's horizontal component around a latitude of 65° can be more than 500 nT over a distance of 167 km. This difference is shown in Figure 9d, and it arises between the two SMA-station locations in (ROS) and Ritsemjokk (RIJ). We cannot assume that the difference between the stations is linearly distributed. If an application requires information on the intensity of the disturbance with an accuracy of less than 500 nT, the station spacing of the magnetometer array used by the application must be less than 200 km. When considering the data measured by the field magnetometer, an external, man-made interference cannot be ruled out. This highlights the importance of observatory quality magnetic measurements and proper data recording methods, for both short- and long-term magnetic environment monitoring.
3. In the vicinity of 65° latitude, the magnetic environment can change rapidly within few minutes. Three-minute changes cannot be estimated in different locations by using the data of the nearest station. The magnetic field's strength can increase in any direction no matter how the field changes at a station located 167 km away. These differences appear in the difference curves of the time derivatives. The largest horizontal difference $\Delta|dH/dt| = 2.8$ nT km^{-1}, see Figure 13, is measured between ROS and RIJ stations. The largest differences in other two directions, see Figures 14 and 15, are $\Delta|dZ/dt| = 3$ nT km^{-1} (ROS-RIJ) and $\Delta|dD/dt| = 5.1$ nT km^{-1} (KIR-RIJ).

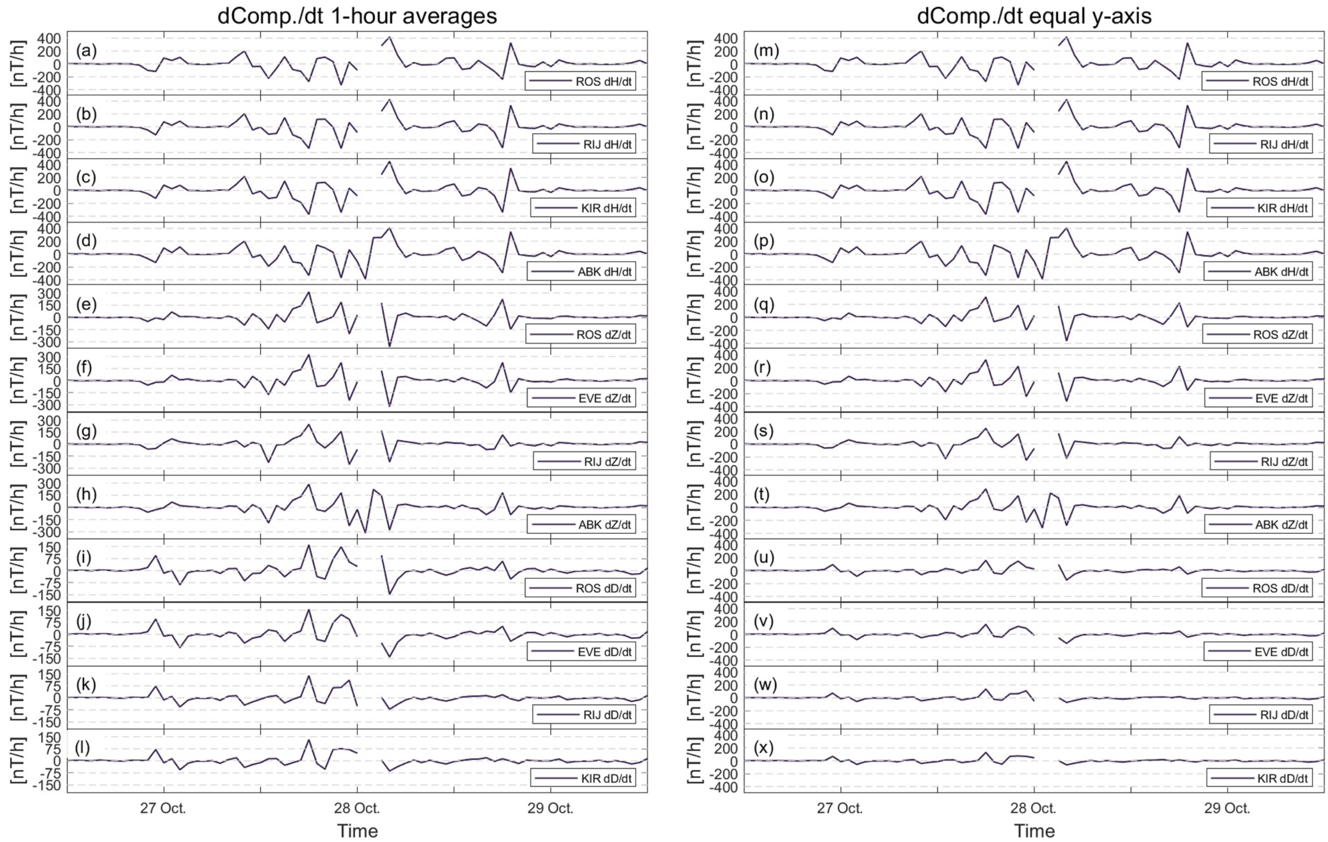

Figure 17. Time derivatives of 1-hr averages. Rostadalen (ROS), Evenes (EVE), Ritsemjokk (RIJ), and Kiruna (KIR) are SMA stations. Abisko (ABK) is a permanent magnetometer station (a–l) Panels allow us to compare the morphology of the storm period and (m–x) panels the amplitude differences.

Acknowledgments
This work was supported by ReSoLVE Center of Excellence funded by the Academy of Finland (projects 272157 and 307411); FLEX-EPOS & G-EPOS infrastructures within EPOS and FIN-EPOS (numbers 293488, 311714, and 328778); and Vilho, Yrjö and Kalle Väisälä Foundation of the Finnish Academy of Science and Letters. The authors thank Markku Mäkelä for the design and construction of the custom-built digitization device DigiMAG. O. Kärhä thanks Pyry Peitso, Mika Väänänen, Tero Raita and Hermann Opgenoorth for helpful conversations and guidance. The authors are grateful for NASA's Space Physics Data Facility for space-borne data. The key persons behind the IMP-8 data sets are Adam Szabo, Ron Lepping, and Norman Ness. The authors thank the geomagnetic observatories Kakioka [JMA], Honolulu and San Juan [USGS], Hermanus [RSA], INTERMAGNET, and many others for their cooperation to make the final Dst index available. The authors are thankful for the Geological Survey of Sweden for maintaining Abisko magnetometer.

Data Availability Statement

Photographs of four studied film reels (19 August 1977 to 02 November 1977 [KIR], 20 August 1977 to 01 November 1977 [RIJ], 22 September 77 to 01 December 1977 [EVE], and 22 September 1977 to 04 December 1977 [ROS]) and digitized numerical values between 26 and 30 October are available at https://doi.org/10.23729/53fd-b1a8-6cb0-40a2-b7a7-d2306948eff4. Photographs were taken by using DigiMAG.

References

Akasofu, S.-I., Kisabeth, J., Romick, G. J., Kroehl, H. W., & Ahn, B.-H. (1980). Day-to-day and average magnetic variations along the IMS Alaska Meridian Chain of observatories and modeling of a three-dimensional current system. *Journal of Geophysical Research*, *85*(A5), 2065–2078. https://doi.org/10.1029/JA085iA05p02065

Akasofu, S.-I., Perreault, P. D., Yasuhara, F., & Meng, C.-I. (1973). Auroral substorms and the interplanetary magnetic field. *Journal of Geophysical Research*, *78*(31), 7490–7508. https://doi.org/10.1029/JA078i031p07490

Akasofu, S.-I., Wilson, C. R., Snyder, L., & Perreault, P. D. (1971). Results from a meridian chain of observatories in the Alaskan sector (I). *Planetary and Space Science*, *19*(5), 477–482. https://doi.org/10.1016/0032-0633(71)90163-2

Araki, T., Shimazu, H., Kamei, T., & Hanado, H. (1992). Scandinavian IMS magnetometer array data and their use for studies of geomagnetic rapid variations. *Proceedings of the NIPR Symposium on Upper Atmosphere Physics*, *5*, 10–20.

Asbridge, J. R., Bame, S. J., Feldman, W. C., & Montgomery, M. D. (1976). Helium and hydrogen velocity differences in the solar wind. *Journal of Geophysical Research*, *81*(16), 2719–2727. https://doi.org/10.1029/JA081i016p02719

Aubry, M. P., & McPherron, R. L. (1971). Magnetotail changes in relation to the solar wind magnetic field and magnetospheric substorms. *Journal of Geophysical Research*, *76*(19), 4381–4401. https://doi.org/10.1029/JA076i019p04381

Bame, S. J., Asbridge, J. R., Felthauser, H. E., Glore, J. P., Paschmann, G., Hemmerich, P., et al. (1978). ISEE-1 and ISEE-2 fast plasma experiment and the ISEE-1 solar wind experiment. *IEEE Transactions on Geoscience Electronics*, *16*(3), 216–220. https://doi.org/10.1109/TGE.1978.294550

Bannister, J. R., & Gough, D. I. (1977). Development of a polar magnetic substorm: A two-dimensional magnetometer array study. *Geophysical Journal International*, *51*(1), 75–90. https://doi.org/10.1111/j.1365-246X.1977.tb04191.x

Baumjohann, W. (1982). Magnetometer networks in northern Europe. In C. T. Russell, & D. J. Southwood (Eds.), *The IMS source book: Guide to the International Magnetospheric Study data analysis* (pp. 134–140). AGU. https://doi.org/10.1029/SP020p0134

Beer, J. H., & Gough, D. I. (1980). Conductive structures in southernmost Africa: A magnetometer array study. *Geophysical Journal International*, *63*(2), 479–495. https://doi.org/10.1111/j.1365-246X.1980.tb02633.x

Burlaga, L. F. (1988). Magnetic clouds and force-free fields with constant alpha. *Journal of Geophysical Research*, *93*(A7), 7217–7224. https://doi.org/10.1029/JA093iA07p07217

Burlaga, L. F., Sittler, E., Mariani, F., & Schwenn, R. (1981). Magnetic loop behind an interplanetary shock: Voyager, Helios, and IMP 8 observations. *Journal of Geophysical Research*, *86*(A8), 6673–6684. https://doi.org/10.1029/JA086iA08p06673

Chapman, S., & Bartels, J. (1940). *Geomagnetism* (1st ed., Vol. 1). ClarendonOUP.

Davis, T. N., & Sugiura, M. (1966). Auroral electrojet activity index AE and its universal time variations. *Journal of Geophysical Research*, *71*(3), 785–801. https://doi.org/10.1029/JZ071i003p00785

Dungey, J. W. (1953). LXXVI. conditions for the occurrence of electrical discharges in astrophysical systems. *The London, Edinburgh, and Dublin Philosophical Magazine and Journal of Science*, *44*(354), 725–738. https://doi.org/10.1080/14786440708521050

Dungey, J. W. (1961). Interplanetary magnetic field and the auroral zones. *Physical Review Letters*, *6*(2), 47–48. https://doi.org/10.1103/PhysRevLett.6.47

Fok, M.-C., Moore, T. E., & Greenspan, M. E. (1996). Ring current development during storm main phase. *Journal of Geophysical Research*, *101*(A7), 15311–15322. https://doi.org/10.1029/96JA01274

Freeman, M. P., Forsyth, C., & Rae, I. J. (2019). The influence of substorms on extreme rates of change of the surface horizontal magnetic field in the United Kingdom. *Space Weather*, *17*, 827–844. https://doi.org/10.1029/2018SW002148

Gonzalez, W. D., Joselyn, J. A., Kamide, Y., Kroehl, H. W., Rostoker, G., Tsurutani, B. T., & Vasyliunas, V. M. (1994). What is a geomagnetic storm? *Journal of Geophysical Research*, *99*(A4), 5771–5792. https://doi.org/10.1029/93JA02867

Gough, D. I., & Reitzel, J. S. (1967). A portable three-component magnetic variometer. *Journal of Geomagnetism and Geoelectricity*, *19*(3), 203–215. https://doi.org/10.5636/jgg.19.203

Grafe, A. (1999). Are our ideas about Dst correct? *Annales Geophysicae*, *17*(1), 1–10. https://doi.org/10.1007/s00585-999-0001-0

Green, C. A. (1981). Continuous magnetic pulsations on the IGS array of magnetometers. *Journal of Atmospheric and Terrestrial Physics*, *43*(9), 883–898. https://doi.org/10.1016/0021-9169(81)90080-5

Gustafsson, G. (1970). A revised corrected geomagnetic coordinate system. *Ark. Geofys.*, *5*, 595–616.

Gustafsson, G. (1984). Corrected geomagnetic coordinates for epoch 1980. In T. A. Potemra (Ed.), *Magnetospheric currents* (pp. 276–283). AGU. https://doi.org/10.1029/gm028p0276

Hamilton, D. C., Gloeckler, G., Ipavich, F. M., Stüdemann, W., Wilken, B., & Kremser, G. (1988). Ring current development during the great geomagnetic storm of February 1986. *Journal of Geophysical Research*, *93*(A12), 14343–14355. https://doi.org/10.1029/JA093iA12p14343

Hayakawa, H., Ebihara, Y., Willis, D., Toriumi, S., Iju, T., Hattori, K., et al. (2019). Temporal and spatial evolutions of a large sunspot group and great auroral storms around the Carrington event in 1859. *Space Weather*, *17*(11), 1553–1569. https://doi.org/10.1029/2019SW002269

Hayakawa, H., Hattori, K., Pevtsov, A., Ebihara, Y., Shea, M., McCracken, K., et al. (2021). The intensity and evolution of the extreme solar and geomagnetic storms in 1938 January. *The Astrophysical Journal*, *990*(2), 197. https://doi.org/10.3847/1538-4357/abc427

Knipp, D. J., Ramsay, A. C., Beard, E. D., Boright, A. L., Cade, W. B., Hewins, I. M., et al. (2016). The May 1967 great storm and radio disruption event: Extreme space weather and extraordinary responses. *Space Weather*, *14*(9), 614–633. https://doi.org/10.1002/2016SW001423

Küppers, F., & Post, H. (1981). A second generation Gough-Reitzel magnetometer. *Journal of Geomagnetism and Geoelectricity*, *33*(3), 225–237. https://doi.org/10.5636/jgg.33.225

Küppers, F., Untiedt, J., Baumjohann, W., Lange, K., & Jones, A. G. (1979). A two-dimensional magnetometer array for ground-based observations of auroral zone electric currents during the International Magnetospheric Study (IMS). *Journal of Geophysics*, *46*(1), 429–450.

Lazarus, A. J., & Paularena, K. I. (1998). A comparison of solar wind parameters from experiments on the IMP 8 and Wind spacecraft. In R. F. Pfaff, J. E. Borovsky, & D. T. Young (Eds.), *Measurement techniques in space plasmas: Particles* (Vol. 102, pp. 85–90). AGU, Geophys. Monogr. Ser. https://doi.org/10.1029/GM102p0085

Loewe, C. A., & Prölss, G. W. (1997). Classification and mean behavior of magnetic storms. *Journal of Geophysical Research*, *102*(A7), 14209–14213. https://doi.org/10.1029/96JA04020

Lühr, H., Thürey, S., & Klöcker, N. (1984). The EISCAT-Magnetometer cross, operational aspects - First results. *Geophysical Surveys*, *6*, 305–315. https://doi.org/10.1007/BF01465545

Maurer, H., & Theile, B. (1978). Parameters of the auroral electrojet from magnetic variations along a meridian. *Journal of Geophysics*, *44*(5), 415–426.

Nevalinna, H. (2006). A study on the great geomagnetic storm of 1859: Comparisons with other storms in the 19th century. *Advances in Space Research*, *38*(2), 180–187. https://doi.org/10.1016/j.asr.2005.07.076

Nose, M., Iyemori, T., Sugiura, M., & Kamei, T. (2015a). *World data center for geomagnetism, Kyoto, geomagnetic AE index*. https://doi.org/10.17593/15031-54800

Nose, M., Iyemori, T., Sugiura, M., & Kamei, T. (2015b). *World data center for geomagnetism, Kyoto, geomagnetic Dst index*. https://doi.org/10.17593/14515-74000

Pellinen, R., Baumjohann, W., & Nielsen, E. (1982). Examples of multi-instrumental studies on auroral phenomena. In C. T. Russell, & D. J. Southwood (Eds.), *The IMS source book: Guide to the international magnetospheric study data analysis* (pp. 124–133). AGU. https://doi.org/10.1029/SP020p0124

Pirjola, R. (1989). Geomagnetically induced currents in the Finnish 400 kV power transmission system. *Physics of the Earth and Planetary Interiors*, *53*, 214–220. https://doi.org/10.1016/0031-9201(89)90005-8

Russell, C. T., McPherron, R. L., & Burton, R. K. (1974). On the cause of geomagnetic storms. *Journal of Geophysical Research*, *79*(7), 1105–1109. https://doi.org/10.1029/JA079i007p01105

Snyder, A. L., & Akasofu, S.-I. (1972). Observations of the auroral oval by the Alaskan meridian chain of stations. *Journal of Geophysical Research*, *77*(19), 3419–3430. https://doi.org/10.1029/JA077i019p03419

Stuart, W. F. (1982). Arrays of magnetometers operated in NW Europe. In C. T. Russell, & D. J. Southwood (Eds.), *The IMS source book: Guide to the international magnetospheric study data analysis* (pp. 141–152). AGU. https://doi.org/10.1029/SP020p0141

Sugiura, M. (1964). Hourly values of equatorial Dst for the IGY. *Annals of the International Geophysical Year*, *35*(9), 5–41.

Tanskanen, E. I. (2009). A comprehensive high-throughput analysis of substorms observed by IMAGE magnetometer network: Years 1993-2003 examined. *Journal of Geophysical Research*, *114*(A05204). https://doi.org/10.1029/2008JA013682

Tanskanen, E. I., Pulkkinen, T. I., Koskinen, H. E. J., & Slavin, J. A. (2002). Substorm energy budget during low and high solar activity: 1997 and 1999 compared. *Journal of Geophysical Research*, *107*(A6), 1086. https://doi.org/10.1029/2001JA900153

Tanskanen, P., Bjordal, J., Block, L., Brønstad, K., Egeland, A., Holtet, T., et al. (1982). SBARMO-79; a multi-balloon campaign in the auroral zone. In C. T. Russell, & D. J. Southwood (Eds.), *The IMS source book: Guide to the international magnetospheric study data analysis* (pp. 153–158). AGU. https://doi.org/10.1029/SP020p0153

Thomson, A. W. P., McKay, A. J., Clarke, E., & Reay, S. J. (2005). Surface electric fields and geomagnetically induced currents in the Scottish Power grid during the 30 October 2003 geomagnetic storm. *Space Weather*, *3*(S11002). https://doi.org/10.1029/2005SW000156

Thomson, D. J., & Weaver, J. T. (1975). The complex image approximation for induction in a multilayered Earth. *Journal of Geophysical Research*, *80*(1), 123–129. https://doi.org/10.1029/JA080i001p00123

Tsyganenko, N. A., Usmanov, A. V., Papitashvili, V. O., Papitashvili, N. E., & Popov, V. A. (1987). *Software for computations of geomagnetic field and related coordinate systems (Tech. Rep.)*. IGY.

Untiedt, J., & Baumjohann, W. (1993). Studies of polar current systems using the IMS Scandinavian magnetometer array. *Space Science Reviews*, *63*, 245–390. https://doi.org/10.1007/BF00750770

Viljanen, A., Nevalinna, H., Pajunpää, K., & Pulkkinen, A. (2001). Time derivative of the horizontal geomagnetic field as an activity indicator. *Annales Geophysicae*, *19*(9), 1107–1118. https://doi.org/10.5194/angeo-19-1107-2001

Walsh, A. P., Haaland, S., Forsyth, C., Keesee, A. M., Kissinger, J., Li, K., et al. (2014). Dawn–dusk asymmetries in the coupled solar wind–magnetosphere–ionosphere system: A review. *Annales Geophysicae*, *32*(7), 705–737. https://doi.org/10.5194/angeo-32-705-2014

Wilson, R. M., & Hildner, E. (1984). Are interplanetary magnetic clouds manifestations of coronal transients at 1 AU? *Solar Physics*, *91*, 169–180. https://doi.org/10.1007/BF00213622